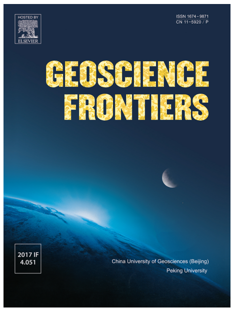

Neoarchean and Rhyacian TTG-Sanukitoid suites in the southern São Francisco Paleocontinent, Brazil: Evidence for diachronous change towards modern tectonics

Henrique Bruno, Vitalino Elizeu, Monica Heilbron, Claudio de Morisson Valeriano, Rob Strachan, Mike Fowler, Samuel Bersan, Hugo Moreira, Ivo Dussin, Luiz Guilherme do Eirado Silva, Miguel Tupinambá, Julio Almeida, Carla Neto, Craig Storey

PII: S1674-9871(20)30038-4

DOI: https://doi.org/10.1016/j.gsf.2020.01.015

Reference: GSF 947

To appear in: *Geoscience Frontiers*

Received Date: 3 September 2019

Revised Date: 2 December 2019

Accepted Date: 26 January 2020

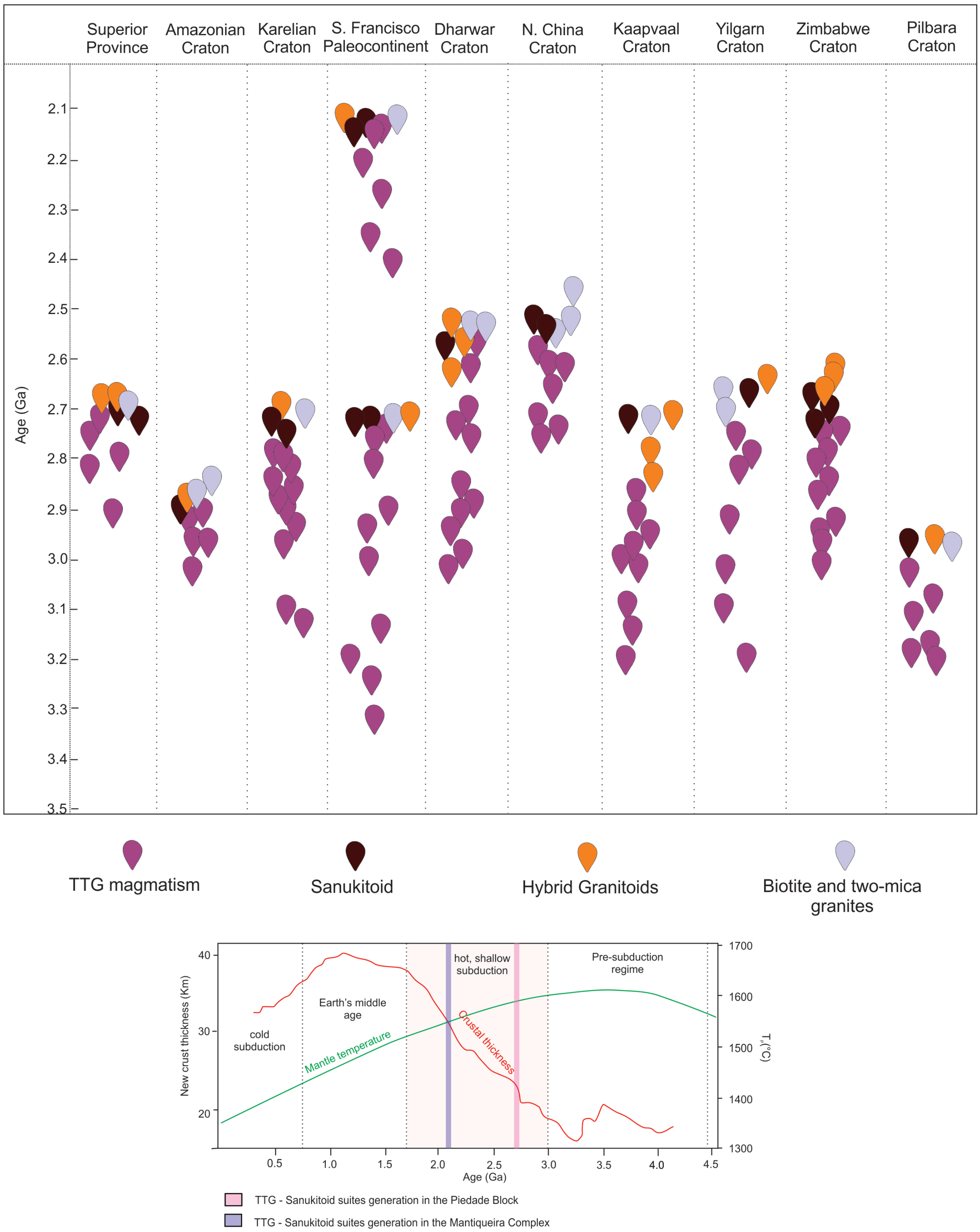
Superior Province
Amazonian Craton
Karelian Craton
S. Francisco Paleocontinent
Dharwar Craton
N. China Craton
Kaapvaal Craton
Yilgarn Craton
Zimbabwe Craton
Pilbara Craton
Age (Ga)
2.1
2.2
2.3
2.4
2.5
2.6
2.7
2.8
2.9
3.0
3.1
3.2
3.3
3.4
3.5
TTG magmatism
Sanukitoid
Hybrid Granitoids
Biotite and two-mica granites
New crust thickness (Km)
40
30
20
cold subduction
Earth's middle age
hot, shallow subduction
Pre-subduction regime
Mantle temperature
Crustal thickness
1700
1600
1500
1400
1300
T_p (°C)
0.5
1.0
1.5
2.0
2.5
3.0
3.5
4.0
4.5
Age (Ga)
TTG - Sanukitoid suites generation in the Piedade Block
TTG - Sanukitoid suites generation in the Mantiqueira Complex

Neoarchean and Rhyacian TTG-Sanukitoid suites in the southern São Francisco Paleocontinent, Brazil: Evidence for diachronous change towards modern tectonics

Henrique Bruno[a,b,*], Vitalino Elizeu[a], Monica Heilbron[a,c], Claudio de Morisson Valeriano[a,c], Rob Strachan[b], Mike Fowler[b], Samuel Bersan[d], Hugo Moreira[b], Ivo Dussin[a], Luiz Guilherme do Eirado Silva[a], Miguel Tupinambá[a], Julio Almeida[a], Carla Neto[a,e], Craig Storey[b]

[a] *Universidade do Estado do Rio de Janeiro, Faculdade de Geologia, Tektos – Grupo de Pesquisa em Geotectônica. Rua São Francisco Xavier 524, Maracanã, Rio de Janeiro, Brazil*

[b] *University of Portsmouth, School of Earth and Environmental Sciences, Burnaby Building, Burnaby Road, Portsmouth, UK*

[c] *Universität Salzburg, Department of Geography and Geology, Kapitelgasse 4-65020 Salzburg, Austria*

[d] *Universidade Federal de Ouro Preto, Departamento de Geologia, Campus Morro do Cruzeiro, Ouro Preto, MG, Brasil*

[e] *Laboratório de Geocronologia e Isótopos Radiogênicos, Universidade do Estado do Rio de Janeiro, Rua São Francisco Xavier 524, Maracanã, Rio de Janeiro, Brazil*

*Corresponding author. E-mail address: henriquebruno.uerj@gmail.com

Abstract

The southern portion of the São Francisco Palaeocontinent in Brazil is denoted by Archean nuclei and Paleoproterozoic magmatic arcs that were amalgamated during Siderian to Orosirian orogenic processes (ca. 2.4–2.1 Ga). New isotopic U-Pb in zircon and Sm-Nd whole rock combined with major and trace element composition analyses constrain the crystallization history of the Neoarchean Piedade block (at ca. 2.6 Ga) and the Paleoproterozoic Mantiqueira Complex (ca. 2.1–1.9 Ga). These therefore display quite different magmatic histories prior to their amalgamation at ca. 2.05 Ga. Sm-Nd and Rb-Sr isotopes imply a mixed mantle-crustal origin for the samples in both units. A complete Palaeoproterozoic orogenic cycle, from subduction to collision and collapse, is recorded in the Piedade Block and the Mantiqueira Complex. Rhyacian to Orosirian subduction processes (ca. 2.2–2.1 Ga) led to the generation of coeval (ca. 2.16 Ga) TTG suites and sanukitoids, followed by late (2.10–2.02 Ga) high-K granitoids that mark the collisional stage. The collisional accretion of the Mantiqueira Complex against the Piedade Block at 2.08–2.04 Ga is also recorded by granulite facies metamorphism in the latter terrane, along the Ponte Nova suture zone. The collisional stage was closely followed by the emplacement of within-plate tholeiites at ca. 2.04 Ga and by alkaline rocks (syenites and enriched basic rocks) at ca. 1.98 Ga, marking the transition to an extensional tectonic regime The discovery of two episodes of TTG and sanukitoid magmatism, one during the Neoarchean in the Piedade Complex and another during the Rhyacian in the Mantiqueira Complex, indicates that the onset of subduction-related melting of metasomatized mantle was not restricted to Neoarchean times, as generally believed , but persisted much later into the Paleoproterozoic.

Keywords: Geodynamics; High Ba-Sr granitoids; Diachronous TTG-sanukitoid transition; Paleoproterozoic; Mantiqueira Complex

1. **Introduction**

The origin of granitoid rocks and of their geochemical signatures have been the subject of many studies and plays an important role in the understanding of the transition from possible shallow subduction in the Archean to steeper subduction plate tectonics in the Paleoproterozoic (Condie and Kröner, 2008; Dhuime et al., 2012; Moyen and Martin, 2012; Korenaga, 2013; Hastie et al., 2016; Tang et al., 2016, Hawkesworth et al., 2016). It is widely accepted that the Archean Proterozoic boundary marks important changes in the geodynamics of the planet (Martin et al., 2005; Windley and Garde, 2009; Martin et al., 2010; Laurent et al., 2014) with the shift between the predominance of Tonalite-Trondhjemite-Granodiorite (TTG) granitoid rocks in the Archean to modern calc-alkaline rocks believed to be marked by the generation of (high Ba-Sr) sanukitoids in the Neoarchean and Paleoproterozoic. High Ba-Sr granitoid rocks are a distinct group of igneous rocks considered to have been formed in subduction settings with significant mantle input (Tarney and Jones, 1994; Fowler et al., 2001, 2008). Thus, their first appearance in the geological record provides important information on the tectonic evolution of the Earth.

Different models have been proposed in the last decades for the genesis of Archean TTG granitoid rocks, such as partial melting of an overthickened eclogitic crust under high pressures (Martin, 1987; Rapp and Watson, 1995; Foley et al., 2002; Rapp et al., 2003; Condie, 2005) and melting of the basaltic portions of subducted slabs (Martin, 1999; Foley et al., 2002). Other authors (e.g. Halla et al., 2009) pointed out that the composition of the TTG series varies widely and that they probably represent a group of rocks with different petrogenetic origins. On the other hand, sanukitoid rocks were mainly emplaced during a period when the dominant mechanism of genesis of the juvenile continental crust changed from Archean melting of hydrous basalts to post-Archean melting of enriched mantle peridotite that underwent metasomatism (Halla, 2005; Kovalenko et al., 2005; Halla et al., 2009; Moyen and Laurent, 2018). According to Martin and Moyen (2002) and Martin et al. (2010), the development of mantle wedges led to interaction between metasomatized mantle and crustally-derived magmas (TTG melt) resulting in sanukitoid melts. The aforementioned changes in the composition of rock associations are believed to reflect the progressive decrease of the mantle temperature, which is thought to have resulted in lower degrees of partial melting of the mantle as well as less melt impregnation within the lithosphere leading to fundamental changes in geodynamic processes (Kemp et al., 2010; Dhuime et al., 2015; Hawkesworth et al., 2016; Tang et al., 2016; Cawood et al., 2018).

The São Francisco Craton (SFC) located in Brazil is a key component of the Gondwana supercontinent and is defined, along with other cratons in Brazil, as comprising a stable crustal segment that was not significantly affected by Neoproterozoic collisional deformation and metamorphism (Almeida et al., 1981; Cordani and Sato, 1999; Campos Neto, 2000; Alkmim et al., 2001; Brito-Neves, 2002) (Fig. 1). The craton is surrounded by Neoproterozoic orogenic belts which in part reworked its peripheral domains (e.g. Heilbron et al., 2017). The term São Francisco Paleocontinent (SFP) is used to denote the amalgamation of Archean nuclei and Paleoproterozoic magmatic arcs during Siderian to Orosirian orogenic processes (ca. 2.4–2.1 Ga) (Trompette, 1994; Noce et al., 2007; Heilbron et al., 2017; Teixeira et al., 2017; Degler et al., 2018; Pinheiro et al., 2019). Therefore, the SFP comprises rock units older than 1.8 Ga, regardless of the intensity of Neoproterozoic overprint. Since it contains a wide range of Archean to Paleoproterozoic granitoid rocks and supracrustal successions (Brito-Neves et al., 1999; Almeida et al., 2000; Teixeira et al., 2000; Schobbenhaus and Brito Neves, 2003;

Barbosa and Sabaté, 2004; Fuck et al., 2008; Alkmim and Martins-Neto, 2012), the SFP is a potentially important area for testing models for crustal evolution and associated magmatism.

In the northeastern and southeastern portions of the SFP (Fig. 1), various Archean terranes are flanked by two Paleoproterozoic orogenic belts, the Eastern Bahia Orogen in the north and the Minas Orogen in the south (Alkmim and Teixeira, 2017; Barbosa and Barbosa, 2017; Teixeira et al., 2017).

The Minas Orogen, which is the focus of this work, encompasses three tectonic domains that are thought to have evolved as Paleoproterozoic magmatic arc systems: the Mineiro Belt, and the Mantiqueira and Juiz de Fora complexes (Fig. 1). The Mantiqueira and Juiz de Fora complexes were subsequently both reworked at high metamorphic grades during the Neoproterozoic Brasiliano orogeny (Heilbron et al., 1998; Silva et al., 2002; Heilbron et al., 2010; Heilbron et al., 2017; Degler et al., 2018; Kuibara et al., 2019). The Mantiqueira Complex comprises banded orthogneisses, the protoliths of which originated in a magmatic arc setting (ca. 2.2 Ga), and as younger (ca. 2.15 Ga) collisional granitoids (Heilbron et al., 2010). Inherited zircon grains and Nd isotopic data indicate an Archean crustal component in the origin of these magmas which likely evolved as a Cordilleran-type arc (Duarte et al., 2004). The Mantiqueira Complex has commonly been grouped with the Piedade Complex to the west, the two being interpreted as essentially the same tectonic unit, with the term Mantiqueira Complex being adopted for all orthogneisses containing mafic lenses and metamorphosed at amphibolite facies during the Brasiliano/Pan-African orogeny in the Neoproterozoic (Machado Filho et al., 1983, Hasuy and Oliveira, 1984; Trouw et al., 1986) (Figs. 1 and 2). The Piedade Complex also has been interpreted variously as Archean to Paleoproterozoic TTG gneisses (Teixeira and Figueiredo, 1996), pre- to syn-collisional granitoids related to the Mineiro Belt (Silva et al., 2002), and as a supracrustal sequence possibly of volcanic origin (Hiraga et al., 2017).

This work presents new whole-rock element composition, zircon geochronological (U-Pb) and whole-rock Thermal Ionization Mass Spectrometry (TIMS) isotope (Rb-Sr, Sm-Nd) data from the Mantiqueira and Piedade complexes. The new data strongly suggest that the two complexes originated as geochemically and isotopically contrasting terranes that were amalgamated during latest Rhyacian (ca. 2.05 Ga) orogenesis. The Piedade Complex originated as an Archean paleocontinental block, whereas the Mantiqueira complex formed as a mainly juvenile Paleoproterozoic magmatic arc. Two episodes of TTG-sanukitoid magma generation are identified: an older event ca. 2.7 Ga, in the Piedade Block, and a younger event at ca. 2.1 Ga in the Mantiqueira Complex. The two TTG-sanukitoid episodes have significant implications for the timing of the change towards modern tectonics.

2. Tectonic framework of the São Francisco Paleocontinent

The Minas and Eastern Bahia orogens (Fig. 1) developed in a similar manner, with accretion of juvenile and continental arcs and related (volcano) sedimentary basins between ca. 2.4 and 2.1 Ga. Final accretionary processes are marked by late collisional granitoid rocks between ca. 2.1 and 2.05 Ga, regional metamorphism at ca. 2.05 to 2.04 Ga, and the development of foreland basins (Teixeira and Figueiredo, 1991; Trompette, 1994; Silva et al., 2002; Barbosa and Sabaté, 2004; Noce et al., 2010, Heilbron et al., 2010; Barbosa et al., 2015; Cruz et al., 2015; Teixeira et al., 2015; Alkmim and Teixeira, 2017; Barbosa and Barbosa, 2017).

The northeastern portion of the SFP, the Eastern Bahia Orogen, was not subjected to Neoproterozoic orogenic reworking, so the Paleoproterozoic terranes and Archean blocks (e.g. Gavião, Guanhães, Serrinha and Jequié), are better preserved than the rocks of the Minas Orogen. The Archean blocks comprise migmatites, granulites, greenstone belts and granitoids which were variably reworked during the Paleoproterozoic (e.g. Barbosa et al., 2012). The Eastern Bahia Orogen comprises a series of tectonic units including the minor Archean blocks and the Paleoproterozoic units: the Western Bahia Magmatic Arc, the Itabuna-Salvador-Curaçá belt (ISAC) and the Buerarema complex (Brito Neves et al., 1999; Barbosa and Barbosa, 2017; Bersan et al., 2018). The Western Bahia Magmatic Arc is interpreted as a Cordilleran-type arc that resulted from melting or reworking of continental crust with some contribution from metasomatized mantle during the collision of the Gavião and Jequié Archean blocks (Cruz et al., 2016; Silva et al., 2016; Aguilar et al., 2017). The ISAC is characterized by the Paleoproterozoic reworking of Archean crust with emplacement of 2.1–2.06 Ga arc-related rocks (Oliveira et al., 2009; Barbosa and Barbosa, 2017; Teixeira et al., 2017), whereas the Buerarema complex is interpreted as a moderately juvenile magmatic arc (ε_{Nd}(2.1 Ga) values +3.1 to −1.7) that was accreted to the Archean nuclei at ca. 2.06 Ga (Silva et al., 2002; Pinho et al., 2011).

In the southern portion of the SFP, the Archean blocks were largely overprinted during Paleoproterozoic orogenesis and are referred to as the Campo Belo, Belo Horizonte and Bonfim metamorphic complexes. They constitute a medium- to high-grade metamorphic terrane mainly composed of TTG suites, migmatites and K-rich granitic plutons, with remnants of supracrustal associations, including typical greenstone belts, and mafic-ultramafic layered bodies (Machado et al., 1992; Pinese et al., 1995; Teixeira et al., 2000; Alkmim and Noce, 2006; Goulart et al., 2013; Lana et al., 2013; Romano et al., 2013; Farina et al., 2015).

The Minas Orogen comprises the Mineiro Belt, and the Piedade, Mantiqueira and Juiz de Fora complexes (Fig. 1). The evolutionary history of the Mineiro Belt is characterized by intrusion of granitoids between 2.47 and 2.12 Ga and successive collisions of oceanic and continental magmatic arcs during the Paleoproterozoic (Ávila et al., 2014; Alkmim and Teixeira, 2017; Moreira et al., 2018; Barbosa et al., 2019), with eventual collision with the Archean continental margin at 2.1 Ga (Teixeira et al., 2015). The Mineiro Belt is mainly composed of orthogneisses, undeformed plutons and volcanic and subvolcanic rocks with juvenile signatures ε_{Nd} (2.2 Ga), suggesting a Paleoproterozoic source with minor crustal contamination (Ávila et al., 2014; Cardoso et al., 2018).

The Juiz de Fora Complex consists mainly of a 2.42–2.08 Ga calc-alkaline suite (Heilbron, et al., 2010) that was metamorphosed to granulite facies during the Ediacaran (Heilbron et al., 1998; Trouw et al., 2000). Most of the authors interpret the Juiz de Fora Complex as the product of subduction-related magmatism in an intra-oceanic environment (Noce et al., 2007; Heilbron et al., 2010).

The Mantiqueira and Piedade complexes, the focus of this work, have been collectively characterized as a Paleoproterozoic Cordilleran arc (Teixeira and Figueiredo, 1991; Brueckner et al., 2000; Silva et al., 2002; Duarte et al., 2004; Noce et al., 2007; Heilbron et al., 2010; Cutts et al., 2018; Degler et al., 2018; Kuibara et al., 2019). The Mantiqueira Complex is characterized by substantial magmatic additions in the time interval of 2.2 to 2.05 Ga and despite the strong Neoproterozoic overprint, a metamorphic episode dated at ca. 2.04 Ga has also been identified (Heilbron et al., 2010).

3. Regional geological context

In this work the Mantiqueira Complex and Piedade Block are interpreted as distinct tectonostratigraphic terranes. Additional supporting data regarding petrogenetic differences between these two terranes are presented and discussed later in this work.

The map of Fig. 2 displays the main geological units which are the focus of this work. The Ponte Nova and Abre Campo shear zones separate the Mantiqueira Complex from, respectively, the Piedade Block and the Juiz de Fora Complex (Haralyi and Hasui, 1982; Alkmim et al., 2006; Noce et al., 2007; Degler et al., 2018). The Abre Campo shear zone is an oblique thrust that is currently interpreted as a Paleoproterozoic suture zone that was reworked during the Neoproterozoic Brasiliano orogeny (Fig. 2; Alkmim et al., 2006; Heilbron et al., 2000, 2004, 2008). The Ponte Nova shear zone juxtaposed rocks of different metamorphic grades during the Neoproterozoic orogeny (Peres et al., 2004). We characterize this shear zone as a suture zone that separates the rocks mapped as related to the Piedade Block from the Mantiqueira Complex.

3.1. Mantiqueira Complex

The foliation of the orthogneisses of the Mantiqueira Complex dips moderately to the southeast, related to the generation of recumbent to open folds (Fig. 2). A well-developed down-dip stretching lineation is associated to consistent kinematic indicators that show top to the NW tectonic transport during the Brasiliano/Pan-African orogeny (e.g. Heilbron et al., 2017) (Fig. 2). Folded and thrusted Neoproterozoic metasedimentary rocks occur interleaved with the orthogneisses, especially in the vicinity of the Abre Campo shear zone. They are represented by (garnet)-biotite gneisses, coarse quartzite layers interbedded with calc-silicate lenses. Near the contact with the Juiz de Fora Complex, the foliation in the orthogneisses is steep to sub-vertical and of mylonitic character, indicating a higher intensity of Neoproterozoic deformation adjacent to the Abre Campo shear zone.

The Mantiqueira Complex is dominated by a banded orthogneiss with migmatitic textures characterized by hornblende-bearing leucosomes surrounded by melanosomes rich in hornblende, biotite and plagioclase (Fig. 3A, B). A ubiquitous centimeter-scale compositional banding in the paleosome and is defined by alternating bands, rich in mafic or felsic mineral phases, respectively. The mineral assemblage comprises hornblende, biotite, plagioclase, quartz with lesser contents of K-feldspar, and accessory titanite, apatite, zircon and opaque minerals (Fig. 4A, B). Textures observed in thin sections are mostly grano-nematoblastic with the foliation defined by preferred orientation of the mafic minerals parallel to compositional banding. Foliated megacrystic granodiorites occur interleaved with the hornblende-bearing orthogneisses. They display megacrysts of pale pink K-feldspar and light gray plagioclase reaching five centimeters in length in a matrix composed of plagioclase, K-feldspar, quartz and biotite (Fig. 3C).

Another abundant lithology is a medium to fine-grained dioritic orthogneiss characterized by K-feldspar, quartz, plagioclase, hornblende and biotite (Fig. 3D, E). The accessory phases are apatite, allanite, opaque and zircon. Foliated light grey orthogneisses also occur with homogeneous texture and lack a conspicuous compositional banding (Fig. 4C, D). The mineral assemblage of this rock type is composed of hornblende with exsolution of opaque minerals along its cleavage, biotite, plagioclase, quartz and K-feldspar. The accessory minerals are apatite, titanite, zircon and opaque minerals. Leucocratic foliated orthogneisses, with granitic to granodioritic composition occur as metric to centimetric layers, with abrupt contacts with the above-mentioned orthogneisses. Besides quartz, K-feldspar and, plagioclase, they contain accessory phases of biotite, zircon and apatite.

3.2. Piedade block

Homogeneous fine-grained biotite leucogneiss and homogeneous mesocratic (hornblende)-biotite gneiss are the main lithotype of the Piedade block (Hiraga et al., 2017). Orthopyroxene-bearing orthogneisses, with protomylonitic to mylonitic textures crop out in a NE–SW strip in the southern segment of the Piedade block, adjacent to the Ponte Nova shear zone (Fig. 2). Clinopyroxene, hornblende, plagioclase, K-feldspar, quartz (Fig. 4E, F) and garnet in the mafic granulites are representative of the main mineralogy with zircon, opaque phases and apatite as common accessory minerals.

3.3. Metabasic rocks

Two different types of metabasic rocks occur in both the Mantiqueira Complex and the Piedade block. One type occurs as centimetric to metric lenses enclosed by the felsic gneisses with locally diffuse to transitional contacts suggesting some magmatic assimilation by the host. The second metabasite type comprises metric to decametric layers of massive to finely banded amphibolite that display sharp contacts with the country orthogneisses (Fig. 3F). The essential mineralogy comprises hornblende, diopside and biotite in minor proportions, plagioclase and quartz, besides opaque phases, titanite, apatite and zircon as accessory minerals (Fig. 4G–J). Titanite and opaque phases are locally more than 5% abundant. Garnet occurs only in larger metabasic bodies.

4. Analytical results

LA-ICPMS U-Pb geochronology, lithogeochemical and radiogenic isotope data were obtained from a range of samples from the Mantiqueira Complex and Piedade Block. U-Pb analyses were performed in the geochronology laboratories of the University of Portsmouth (UK) and the Ouro Preto Federal University (Brazil); element composition analyses were carried out by Activation Laboratories Ltd (Actlabs, Ancaster, Canada);

and the Sm-Nd and Sr isotope data were acquired by the Laboratory of Geochronology and Radiogenic Isotopes (LAGIR) of the Rio de Janeiro State University (Brazil).

The analytical procedures of the several techniques and laboratories involved in this work can be found in Supplementary Material A.

4.1. U-Pb geochronology

Following geochemical analysis, zircon LA-ICPMS U-Pb geochronology data were obtained from sixteen samples which covered the range of different geochemical signatures across a wide geographical area. In order to select the spots for analysis, cathodoluminescence and secondary electron scanning electron microscopy (SEM) imagery was used. Tables with analytical results are provided in Supplementary Material B.

Geochronology results, summarized in Table 1, fall into two main groups: (1) six samples of the Piedade Block yielded Neoarchean (~2.7 Ga) crystallization ages with evidence for subsequent Rhyacian metamorphism (~2.05 Ga), and in one sample (19A) Ediacaran (~550 Ma) metamorphism; (2) ten samples of the Mantiqueira Complex yielded Rhyacian (~2.1 Ga) crystallization ages overprinted by Ediacaran (~550 Ma) metamorphism.

4.1.1. Neoarchean Piedade Block

Sample 66A was collected from one of the felsic orthogranulite lenses within the Ponte Nova shear zone (Fig. 2). It contains zircon grains that vary from translucent to opaque, with light to deep brown colors. The most common morphology is prismatic (euhedral to subhedral) with few rounded grains. They display fine igneous oscillatory zoning in the cores surrounded by homogeneous bright rims. A few grains show indentation between cores and rims (Fig. 5A). The results are complex with fifty-nine spots divided into cores and rims defining two discordia lines. The analysis of the cores yielded an upper intercept at 2693 ± 23 Ma, interpreted as the age of crystallization of the igneous protoliths, whereas the discordia provided by the analysis of the rims indicates an upper intercept at 2043 ± 30 Ma, interpreted as the age of granulite facies metamorphism (Fig. 6A).

The results of sample 66B, a basic granulite collected in the same outcrop as sample 66A, are complex with forty-four analyses of cores and rims that define two discordia lines (Fig. 5B). Recrystallized, re-homogenized and partly resorbed cores are also present. The grains are mostly subhedral with some sub-rounded, translucent to opaque, varying from light to dark brown colors. The discordia provided by the spots located in cores yielded an upper intercept of 2710 ± 32 Ma, interpreted as the age of crystallization of the igneous protoliths, whereas the discordia resulting from the rims analyses shows an upper intercept of 2067 ± 82 Ma, which is interpreted as the age of metamorphism (Fig. 6B).

Sample 21A was collected from a basic granulite lens in the northern Ponte Nova shear zone (Fig. 2). Zircons display magmatic oscillatory zoning and homogeneous portions in the rims, with some clearly showing inherited cores and igneous rims (Fig. 5C). The data yielded two discordias. Ninety-four analyses define one discordia with an upper intercept at 2690 ± 7.9 Ma, which is interpreted as inheritance. Since the thirty-five analysed grains that define the second discordia display fine igneous oscillatory zoning the upper intercept of 2523 ± 28 Ma is interpreted as the igneous crystallization age (Fig. 6C).

Sample 21B, an intermediate granulite, collected in the same outcrop as sample 21A, displays mostly subhedral to round, translucent to opaque, and light pink to brown zircon grains (Fig. 5E). Four analyses of different grains provided a concordia age of

3045 ± 26 Ma which is interpreted as the age of an inherited component. Fifty-four analyses scatter along the concordia, a feature interpreted as resulting from continuous lead loss during granulite facies metamorphism. The minimum crystallization age of the igneous protolith is constrained at 2731 ± 24 Ma, by the $^{207}Pb/^{206}Pb$ age of spot #10 in an igneous core. The youngest concordant zircon, with a $^{207}Pb/^{206}Pb$ age of 2039 ± 16 Ma (spot #49) is interpreted as the best approximation of the metamorphic age (Fig. 6D).

The zircon population of sample 148, a felsic granulite collected further north along the Ponte Nova shear zone, comprises euhedral to subhedral grains (Fig. 5E), translucent to opaque, with colours varying from light to dark brown. A series of analyses are scattered along Concordia (Fig. 6E). Forty-one concordant analyses scatter between a minimum igneous crystallization age as interpreted from a zoned grain with magmatic oscillatory zoning with a $^{207}Pb/^{206}Pb$ age of 2659 ± 23 Ma (spot #14), and an interpreted metamorphic age of 2085 ± 38 Ma ($^{207}Pb/^{206}Pb$ age) (in the spot #49) (Fig. 6E).

Sample 19A is an intermediate granulite collected from within the Piedade Block. It displays subhedral grains mostly translucent, varying from light to dark brown colours (Fig. 5F). Nineteen analyses yield an upper intercept of 2715 ± 11 Ma, interpreted as the igneous crystallization age and a lower intercept of 592 ± 12 Ma, interpreted as indicative of the age of the Neoproterozoic (Brasiliano/Pan-African orogeny) metamorphic overprint (Fig. 6F).

One hundred and thirty-nine analyses were made from zircons of sample 19B, a basic granulite lens from the same outcrop as sample 19A, that yielded euhedral to subhedral grains, translucent to opaque, varying from light to dark brown (Fig. 5G). The analyses resulted in four different discordias with upper intercepts at 3083 ± 20 Ma, 2617 ± 20 Ma, 2096 ± 33 and 1966 ± 7 Ma. Since the cores and homogeneous zones give the older ages and the younger display fine igneous oscillatory zoning, we interpret the age of 1966 ± 7 Ma, yielded by the youngest upper intercept, as the crystallization age (Fig. 6G).

4.1.2. Paleoproterozoic Mantiqueira Complex

Sample 08, a hornblende biotite gneiss collected in the east of the Mantiqueira Complex (Fig. 2), displays prismatic, euhedral to subhedral zircon grains with fine igneous oscillatory zoning in the cores surrounded by homogeneous bright rims (Fig. 7A). The data from thirty-three analyses define an upper intercept of 2168 ± 21 Ma, interpreted as the igneous crystallization age and a lower intercept of 584 ± 14 Ma, interpreted as the metamorphic overprint. Five analyses of zircon rims yielded a concordia age of 579.2 ± 5.1 Ma with 89% of concordance (Fig. 8A).

Sample 67 is a biotite gneiss that displays prismatic zircon grains with fine igneous oscillatory zoning in the cores surrounded by homogeneous bright rims (Fig. 7B). Thirty-two analyses yielded a discordia with an upper intercept of 2117 ± 28 Ma, interpreted as the igneous crystallization age and a lower intercept of 553 ± 75 Ma that dates the Ediacaran metamorphic overprint (Fig. 8B).

Sample 163A is an orthopyroxene-hornblende-biotite gneiss, and displays subhedral to round, translucent to opaque, and light pink to brown zircon grains (Fig. 7C). Eighty analyses yielded a discordia with an upper intercept of 2116 ± 15 Ma and a lower intercept of 569 ± 12 Ma interpreted as, respectively, igneous crystallisation and metamorphic overgrowth ages (Fig. 8C).

Sample 137G is a hornblende-biotite gneiss collected in the northern part of the Mantiqueira Complex, close to the Abre Campo shear zone. The sample displays colorless to bright yellow colors, subhedral to rounded zircon grains with magmatic oscillatory zoning in the cores and bright metamorphic rims (Fig. 7D). The sample yielded a discordia with fifty-eight analyses showing an upper intercept age of 2023 ± 13 Ma, interpreted as the igneous crystallization age and a lower intercept of 584 ± 14 Ma interpreted as the metamorphic age (Fig. 8D).

Sample 64A is a hornblende-biotite gneiss collected south of the Ponte Nova shear zone. The sample yielded thirty-four analyses from prismatic to subhedral zircon grains with magmatic oscillatory zoning in the cores and bright metamorphic rims (Fig. 7E) that regress on a discordia with an upper intercept at 2016 ± 27 Ma and a lower intercept at 563 ± 24 Ma, respectively interpreted as the ages of igneous crystallization and metamorphism. Three analyses of zircon rims yielded a concordia age of 577 ± 18 Ma (Fig. 8E), which is coincident with the age of metamorphism above.

Zircons from sample 64B, a hornblende biotite gneiss collected in the same outcrop as sample 64A, share the same characteristics of the latter (Fig. 7F).The sample displays a discordia of twenty-nine analyses with an upper intercept age of 2107 ± 17 Ma, thought to represent the igneous crystallization age and a lower intercept age of 567 ± 41 Ma, interpreted as the Ediacaran metamorphism (Fig. 8F).

Zircon grains from Sample 355, a hornblende-biotite gneiss, are prismatic, euhedral to subhedral, translucent colourless to bright brown colours (Fig. 7G). Forty analyses define a discordia with an upper intercept of 1983 ± 13 Ma and a lower intercept of 557 ± 14 Ma, respectively interpreted as indicating igneous crystallization and metamorphism (Fig. 8G).

Zircon grains from amphibolite sample 103C are translucent to opaque prismatic, euhedral to subhedral grains with light brown colours (Fig. 7H). One hundred analyses regress on discordia to yield an upper intercept of 2044 ± 6 Ma and a lower intercept of

661 ± 64 Ma, respectively interpreted as igneous crystallization and metamorphic ages (Fig. 8H).

Sample 70D, an amphibolite collected close to the Abre Campo shear zone, displays subhedral to rounded zircon grains with magmatic oscillatory zoning in the cores and bright metamorphic rims, with colorless to bright brown colors (Fig. 7I). Thirty-nine analyses regress on discordia to yield an upper intercept of 1989 ± 13 Ma interpreted as the igneous crystallization age and a lower intercept of 610 ± 33 Ma, interpreted as the Neoproterozoic metamorphic overprint (Fig. 8I).

4.2. Geochemistry and isotope data

Twenty-nine samples were selected for major and trace element composition analyses: seven from the Piedade Block and twenty-two from the Mantiqueira Complex. Twelve samples were selected for radiogenic isotope analyses based on their geochemical affinities: four from the Neoarchean Piedade Block and eight from the Rhyacian Mantiqueira Complex. Four compositional groups of felsic and intermediate rocks and two compositional groups of basic rocks have been selected based on their geochemical affinities.

4.2.1. High Ba-Sr granitoids

All the intermediate and felsic rocks plot in the calc-alkaline series on the AFM diagram (Fig. 9A), and are classified as high Ba-Sr granitoids (Fig. 9B), following the characteristics described by Tarney and Jones (1994), Fowler et al. (2001), and Fowler et al. (2008). They are characterised by: (1) high Ba, Sr, light-REE and K/Rb ratios, and low Rb, Th, U, Nb, Ta and Y and heavy-REE (Tables 2–4); (2) lack of a pronounced negative Eu anomaly; (3) a marked negative Nb anomaly.

The first compositional group is present in both the Piedade Block and Mantiqueira Complex. It is characterized as silica-rich (SiO_2> 62 wt.%), with high Na_2O contents (3.3–4.5 wt.% Na_2O), and therefore low K_2O/Na_2O (<0.5) and is poor in ferromagnesian elements (Fe_2O_3, MgO, MnO, TiO_2) (Table 2). In the TAS diagram (Fig. 10A) these rocks plot in the granodiorite and granite fields, due to high SiO_2 contents. In the SiO_2 vs. K_2O diagram (Fig. 10B), the samples plot on the medium-K calc-alkaline field and are also classified as calcic, magnesian and slightly peraluminous to metaluminous (Fig. 11). In the REE chondrite-normalized diagram, the group shows high light rare earth element (LREE), low heavy rare earth element (HREE) and positive Eu anomalies (Fig. 12A). In the primitive mantle diagram (Fig. 12B), the samples have peaks at Ba, Pb and Zr and troughs at P, Nb and Th.

The second compositional group is also present in both the Piedade Block and Mantiqueira Complex. This group plots in the intemediate field (diorite) of the TAS diagram (Fig. 10A) with SiO_2 contents varying from 57.9–61.8 wt.% (Table 3). In the SiO_2 vs. K_2O diagram, the samples plot in the medium-K calc-alkaline field (Fig. 10B) and are characterized as calcic to alkali-calcic, magnesian and metaluminous ($0.7 \leq$ A/CNK ≤ 1.0) (Fig. 11). They are high in ferromagnesian oxides ($5 \leq FeO^t + MgO + MnO + TiO_2 \leq 25$ wt.%) and CaO (Table 3). All the samples have higher concentrations in compatible trace elements Ni and Cr and in incompatible elements (K_2O= 1.1–1.90 wt.%, Ba = 544–892 ppm and Sr = 288–379 ppm). The samples show high Mg# (37–48) for their silica content. The chondrite-normalized REE patterns show enrichment in LREE relative to HREE and small negative Eu anomalies (Fig. 12C). In the primitive mantle diagram, all the samples show enrichment in fluid-mobile large-ion lithophile elements (Ba, Rb and K) and Pb (Fig. 12D).

The third compositional group occurs only in the Mantiqueira Complex. It shares many geochemical similarities with the second group described above but has some important differences such as lower contents of SiO_2 (wt.%), lower Mg# and compatible elements (such as Ni and Cr) and higher LREE (Table 4). In the TAS diagram the samples plot at the boundary between the subalkaline/tholeiitic and alkaline series (Fig. 10A). In the SiO_2 vs. K_2O diagram (Fig. 10B) they plot in the high-K calc-alkaline series, and are classified mostly as ferroan, alkali-calcic and metaluminous granitoids (Fig. 11). In the chondrite-normalized REE diagram (Fig. 12E), the samples are enriched in LREE, and have relatively low HREE and negative Eu anomalies. In the primitive mantle diagram (Fig. 12F), the group displays characteristics of late to post-collisional granitoids with high contents of Zr, Ce, Nb and Y (Table 4).

Sample 355 of the Mantiqueira Complex is significantly different and therefore represents a single member of a fourth compositional group (Table 4). It displays high contents of K_2O (7.4 wt.%) and other incompatible elements (Ba 3891 ppm, Sr 1350 ppm) together with a high K_2O/Na_2O ratio (2.93), high Mg# (53), Ni and Cr. (Table 4). In the TAS diagram, the sample plots in the syenite field of the alkaline series (Fig. 10A), Chondrite-normalized REE patterns shows more abundant LREE than the other groups, and relatively low HREE (Fig. 12G). In the primitive mantle diagram, there is clear enrichment in fluid-mobile large-ion lithophile elements (Ba, Rb and K) and a negative Ti anomaly (Fig. 12H).

4.2.2. Metabasic rocks

The basic rocks are subdivided into two compositional groups (Table 5), present in both the Piedade Block and Mantiqueira Complex, taking into consideration their TiO_2 and REE patterns and differences in the Al_2O_3, K_2O and Na_2O contents and crystallization ages (Table 5). All samples are classified as tholeiitic in an AFM diagram (Fig. 9A).

Group 1, on the TAS diagram, plot in the gabbro field at the boundary between the subalkaline/tholeiitic and alkaline and Group 2 also plot in the gabbro field but in the subalkaline/tholeiitic series.

In the chondrite-normalized REE diagrams, samples from Group 1 have a fractionated pattern with high LREE and a discrete negative Eu anomaly (Fig. 13A) suggesting a within-plate alkaline basalt (WPAB), whereas samples from Group 2 have flat patterns with slight enrichment in LREE suggesting an E-MORB affinity (Fig. 13B).

In the N-MORB-normalized diagram, samples of Group 1 (Fig. 13C) have positive anomalies in Ba, Pb and Nd, whereas patterns from Group 2 (Fig. 13D) show enrichment in Ba, K, Pb and Nd. Group 1 displays a transitional character mostly because of high alkali metal and LILE (Rb and Ba) with increasing OIB components (Zr/Nb < 20) (Table 5). Group 2 has an E-MORB (Enriched mid-ocean ridge basalt) signature with enrichment in incompatible elements such as K, B, La and Rb (Table 5).

4.2.3 . Sm-Nd and Sr isotopes

The Sm-Nd and Sr isotopic results are shown in Table 6. The Neoarchean samples of the Piedade Block have $\varepsilon_{Nd}(t)$ values between -2.5 and -5.4 at their respective crystallization ages. Their initial $^{87}Sr/^{86}Sr$ ratios range from 0.7031 and 0.7069 and initial $^{143}Nd/^{144}Nd$ ratios vary from 0.5090 and 0.5091. In the Paleoproterozoic samples of the Mantiqueira Complex, the $\varepsilon_{Nd}(t)$ values vary between +1.6 and -9.7 at their respective crystallization ages. Initial $^{87}Sr/^{86}Sr$ ratios range from 0.7019 and 0.7070 and initial $^{143}Nd/^{144}Nd$ ratios vary from 0.5093 to 0.5102 (Table 6). In the $\varepsilon_{Nd}(t)$ vs. crystallization age diagram shown in Fig. 14, the striking differences between the source of the Paleoproterozoic and Archean rocks is evident, without overlap with the field representing the isotope evolution of the Archean São Francisco Paleocontinent (Teixeira et al., 1996).

5. Discussion

5.1. Petrogenetic evolution

Some authors propose that the generation of sanukitoids represent the transition between the generation of TTGs by melting of hydrous basalt to the modern production of calc-alkaline granitoid rock (Shirey and Hanson, 1984; Martin et al., 2009; Heilimo et al., 2010). This change occurred preferentially across the Archean-Paleoproterozoic boundary (Laurent et al., 2014; Moyen and Laurent, 2018). Because of the wide geochemical diversity of TTGs, different geodynamic models have been proposed for their generation: (1) subduction of meta-basalts which undergo melting due to presumably higher Archean geothermal gradients; (2) non-subduction settings through the progressive melting of a thick oceanic plateau above a long-lived mantle plume (i.e. stagnant lid) (e.g. Bédard, 2006) and (3) delamination at the base of a magmatically or tectonically over-thickened mafic crust. (e.g. Moyen and Laurent, 2018);

The proposed mechanism for the origin of sanukitoids is the opening of the mantle wedge after a period of shallow subduction promoting interaction between metasomatized mantle and crustal derived magmas. Subduction (with viable subduction angle) is a suitable tectonic setting for enrichment of crustal elements in the asthenospheric mantle, which is regarded as the source of the sanukitoid magmas (Heilimo et al., 2010; Laurent et al., 2014; Rajesh et al., 2018). The generation of sanukitoid magma is driven by interaction between mantle peridotite and LILE and LREE-rich fluids or melts, since the melting of delaminated basalts (i.e. delamination of the lower crust in a stagnant lid system) alone would not be rich enough in incompatible elements and water to achieve the observed enrichment (Kovalenko et al., 2005; Lauren et al., 2014). Many authors propose that the mantle source of the sanukitoids included sediments or sediment-derived fluids, by a two-stage model where the lithospheric mantle wedge is enriched during subduction by melts/fluids from the descending slab and sediments followed by a metasomatism caused by upwelling of the asthenospheric mantle. (e.g. Heilimo et al., 2010; Laurent et al., 2014).

This critical change in global geodynamics has been suggested to have taken place in the late Archean based on parameters such as crystallization age of the relevant rocks, the thickness, temperature and rheology of oceanic and continental crust and the increase in the global volume of continents (e.g. Laurent et al., 2014). According to this model, all late Archean granitoids would have been formed as the result of different degrees of interaction between two end members: (a) the local continental crust and (b) mantle peridotite metasomatically enriched in incompatible elements.

TTGs and sanukitoids have been recognized in this work, in both the Piedade Block and the Mantiqueira Complex. The TTG rocks were classified using the criteria of Moyen and Martin (2012), as calc-alkaline rocks, metaluminous to slightly peraluminous, silica rich magmatic rocks, low contents of ferromagnesian oxides, low K_2O/Na_2O ratios. Thus, the sanukitoid rocks were classified according to Martin et al. (2005), Heilimo et al. (2010), Martin et al. (2010), Laurent et al. (2014), as calc-alkaline rocks, metaluminous, large range of silica content, high contents of ferromagnesian oxides, variable K_2O contents, rich in Ba and Sr, high magnesium number, high contents in transition elements such as V, Ni and Cr.

TTG samples plot in the designated TTG field in the La/Yb vs. Yb diagram (Fig. 15A) and on the normative feldspar classification diagram for granitoids (Fig. 15B). In the petrogenetic indicator diagram of Laurent et al. (2014) (Fig. 15C) in which each end member represents a geochemical reservoir possibly related to the chemistry of the granitoids, the Na_2O/K_2O end member represents melting of meta-igneous mafic rocks with low to moderate K_2O contents, the A/CNK end member representing the pre-existing crustal rocks and the FMSB end member represents interaction between the peridotite and components rich in incompatible elements. In the ternary diagram of figure 16d of Laurent et al. (2014), the composition of melts derived from a potential source is discriminated. The TTG group samples plot in the field characterized as the product of melting of low-K mafic rocks, while the sanukitoid group samples plot in the field of melting of high-K mafic rocks. The TTGs are Sr-rich and Y-HREE-poor and classified in the “low-HREE” group of Halla et al. (2009), as well as in the “medium- to high-pressure” groups of Moyen et al. (2011) suggesting that the generation of these magmas requires the introduction of hydrous mafic rocks into the mantle, implying that they formed in a subduction-like setting (Laurent et al., 2014).

The global transition between the formation of TTGs and sanukitoids in other cratons took place in the Archean (Laurent et al., 2014). However, in the Mineiro belt, a 'delayed' Paleoproterozoic transition was reported by Moreira et al. (2018). Our new data show that, rather than a simple delay, there were two successive TTG-sanukitoid transitions in the São Francisco Paleocontinent: the first in the Piedade Block during the Neoarchean at 2.7–2.6 Ga and the second in the Rhyacian (at ca. 2.1 Ga) in the Mantiqueira Complex. It is highlighted that these two complexes were amalgamated at ca. 2.05 Ga, as suggested by the widespread metamorphic ages recorded in the Piedade Block, implying independent previous tectono-magmatic evolutions.

Based on Sm-Nd and Rb-Sr isotope constraints, the Paleoproterozoic samples may represent a phase of juvenile addition with minor crustal contamination during the build-up of the São Francisco Paleocontinent. In comparison with Neoarchean samples of the Piedade Block, the Paleoproterozoic samples of the Mantiqueira Complex display higher $^{143}Nd/^{144}Nd$ ratios and therefore less negative ε_{Nd} values (Table 6).

In the Sr evolution diagram of Ben Othman et al. (1984) (Fig. 16A), the pink polygon represents the field of the Archean samples, with mixed crustal-mantle origin, as their evolution starts above the line of new continental crust growth, therefore, they may represent reworking of pre-existing continental crust, as also indicated by the presence of inherited zircons. In contrast, the Paleoproterozoic samples plot below the line of evolution of the continental crust and above the mantle curve. Thus, the Paleoproterozoic samples imply an Archean/Paleoproterozoic mantle source followed by contamination with the continental crust. This indicates that, in the Piedade block, the Neoarchean rocks are mostly derived from an evolved source, suggesting contamination from older crust and the Rhyacian magmatism, in the Mantiqueira Complex, is characterized as having a mantle-derived composition with partial crustal contamination.

Specifically, the $^{143}Nd/^{144}Nd$ (initial) vs. $^{87}Sr/^{86}Sr$ (initial) diagram of Fig. 16B shows the isotopic signature of both groups at their crystallization ages. The two groups plot in different fields indicating that they had different origins. In the ε_{Nd} (crystallization ages) vs. $^{87}Sr/^{86}Sr$ (initial) diagram (Fig. 16C), the mixed mantle-crustal origin for the samples both in the Piedade block and in the Mantiqueira Complex are highlighted.

In the diagram showing variation of crustal thickness and mantle temperature through geologic time (Hawkesworth et al., 2016), five stages of Earth's evolution are recognized (Fig. 17). The transition of TTG to sanukitoid magmatism is considered as belonging to the third stage, beginning at ca. 3.0 Ga and lasting until ca. 1.7 Ga. This transition is interpreted to reflect cooling of the Earth, with stabilization of cratons and increasing crustal thickness, allowing subduction driven tectonics to take place (Sizova et al., 2010).

Combining the petrological information with the crystallization age of the Piedade and Mantiqueira samples, we have defined two episodes of transition between TTG and sanukitoid magmatism in the SFP. The older TTG-sanukitoid transition episode took place in the Piedade Block during the Neoarchean (ca. 2.7 Ga), as expected and observed in several cratonic areas of the world (Fig. 18). However, a younger TTG-sanukitoid transition episode was characterized in the Mantiqueira Complex during the Rhyacian (ca. 2.10 Ga), showing that this process can be diachronous, as reported by Moreira et al. (2018) (Fig. 18).

The whole-rock isotopic information presented above, also evident from elemental data, confirms that two different reservoirs, i.e. crust and mantle, are required to generate each magmatic assemblage. Therefore, the data preclude the possibility that the same reservoirs generated the Piedade and Mantiqueira rocks during the Neoarchean and Rhyacian, but rather that two different source assemblages generated TTG and sanukitoids through time. As described by Laurent et al. (2014) in other cratonic blocks around the world, in the southern SFP both TTG-sanukitoid generation episodes were also driven by broadly the same sequence of events: an early period of exclusively TTG magmatism is followed by a shorter stage during which both TTG and sanukitoid rocks are generated together (Fig. 18).

5.2. Tectonic evolution and regional correlations within the Rhyacian orogen of the São Francisco paleocontinent

The new geochronological and lithogeochemical data allow the proposition of an integrated tectonic model that explains the magmatic evolution of the Piedade Block and the Mantiqueira Complex.

In the Piedade Block, the coeval TTG (2.71 Ga) and sanukitoid (ca. 2.69 Ga) magmatism represents the preserved part of the orogen that formed this Neoarchean block. Both are the likely product of mafic crust subduction beneath an older microcontinent, as suggested by inherited zircons and Nd-Sr isotope signatures typical of contaminated magmas. The generation of within-plate alkaline mafic rocks at ca. 2.5 Ga suggests an extensional tectonic regime during this period, supporting the presence of a stable landmass.

Following the model proposed by Heilbron et al. (2010), the Mantiqueira Complex hosts calc-alkaline arc-related banded orthogneisses (ca. 2.2 Ga) and collisional granitoid associations (ca. 2.15 Ga). The coeval TTG and sanukitoid rocks (ca. 2.1 Ga) are interpreted as the collisional stage of an eastward-directed subduction system (Fig. 19A). The westward-directed subduction beneath the Mantiqueira Complex is suggested by Heilbron et al. (2010) to explain the geographic distribution of the geochemical signature in part of the orogenic system. The collisional stage is followed by late (2.10–2.02 Ga) high-K granitoid rocks (Fig. 19B). The granulite facies metamorphic event at ca. 2.05 Ga is thought to represent the accretion of the Piedade Complex to the Mantiqueira Complex coeval with the collision of the latter with the Juiz de Fora Complex (Heilbron et al., 2010).

The within-plate tholeiite magmatism (ca. 2.04–2.0 Ga) represents the transition to an extensional environment in the Mantiqueira Complex, while the ca. 1.9 Ga within-plate alkaline basic rocks with OIB-like signature and the alkaline syenitic sample at ca. 1.9 Ga indicate the beginning of collapse of the orogen (Fig. 19C).

The correlations presented here reflect a possible connection between the Minas Orogen in southern SFP and the Eastern Bahia Orogen located in the northeast SFP during the Paleoproterozoic (Fig. 1). Based on the available geochronological and isotope data, the juvenile to slightly contaminated signatures of the Rhyacian High Ba-Sr rocks of the Mantiqueira Complex are correlatives of the granitoid suites of the Itabuna-Salvador-Curaçá Belt (ISAC) (e.g. Conceição et al., 2003; Oliveira, 2004; Peucat et al., 2011; Barbosa and Barbosa, 2017; Fig. 20). The rocks of the Piedade Block, metamorphosed to granulite facies in the Rhyacian, are similar to the granulitic rocks described within the Jequié Block (Fig. 20; Barbosa and Barbosa, 2017). Both units preserve the same sequence of tectonic events (Silva et al., 2002; Barbosa and Sabaté 2004; Barbosa et al., 2012): (1) a concentration of crystallization ages of the granitoid rocks between ca. 2.8 and 2.7 Ga; (2) gabbroic intrusions around ca. 2.52 Ga; and (3) a pervasive granulite facies overprint between 2.06 and 2.04 Ga, related to the final amalgamation of the Archean landmasses. Sm-Nd T_{DM} model ages for the Jequié rocks range from 3.3–2.9 Ga and the negative $\varepsilon_{Nd}(t)$ values suggest these magmas were generated by reworking of Mesoarchean crust (Marinho et al., 1994a, b; Barbosa and Sabaté, 2004).

The long age interval (ca. 2.2–2.04 Ga) of arc-related granitoid rocks generation in the Mantiqueira Complex and in the ISAC suggests the development of a large magmatic arc system with intervening small Archean continental blocks. Although Archean Nd T_{DM} ages and inherited zircons are documented by Barbosa et al. (2008), Heilbron et al. (2010), and Oliveira et al. (2010), significant juvenile addition took place in the Mantiqueira Complex, as indicated by the U-Pb, Sm-Nd and Rb-Sr isotope data presented herein. The generation of late collisional to post tectonic syenitic and High-K granitoid rocks at ca. 2.08–2.04 Ga (Rosa et al., 2001; Oliveira, 2004) was recorded in both regions.

6. Conclusions

(1) The Neoarchean rocks of the Piedade Block (~2.7 Ga) represent reworking of pre-existing continental crust, as shown by Sm-Nd T_{DM} ages of 2.98–2.96 Ga and by the presence of inherited zircons. Within-plate alkaline basaltic rocks with OIB signature intruding these rocks at 2.5 Ga also suggests the presence of a stable landmass by the end of the Archean.

(2) In the southern São Francisco Paleocontinent, a complete orogenic cycle, from subduction to collision and collapse, was recorded in the Piedade Block and the Mantiqueira Complex. Rhyacian to Orosirian subduction processes (ca. 2.2–2.1 Ga) led to the generation of coeval (ca. 2.16 Ga) TTG suites and sanukitoid rocks, followed by late (2.10–2.02 Ga) high-K granitoids that mark the collisional stage. This collisional stage reflects the accretion of the Mantiqueira Complex against the Piedade Block at 2.08–2.04 Ga as recorded by granulite facies metamorphism in the latter terrane, along the Ponte Nova shear zone. The collisional stage was closely followed by the emplacement of within-plate tholeiites at ca. 2.04 Ga and by alkaline rocks (syenites and enriched basic rocks) at ca. 1.98 Ga, marking the transition to an extensional tectonic regime.

(3) The discovery of two episodes of TTG and sanukitoid rock generations, one during the Neoarchean in the Piedade Block and another during the Rhyacian in the Mantiqueira Complex, indicates that the onset of subduction-related melting of metasomatized mantle was not restricted to Neoarchean times, as previously thought, but persisted much later in the Paleoproterozoic. This discovery opens a new potential line of investigation of diachronous changes in geodynamic regimes within other Paleoproterozoic belts worldwide.

Acknowledgements

The authors thank the facilities and the help from all the technical support of the laboratories (LGPA, LAGIR) of the Geology Institute at UERJ, the Rio de Janeiro State University. We would also like to thank our partners from universities in Brazil (USP, UNB, UFOP) and abroad (UQAM and Edmonton, Canada; Portsmouth, UK; Notre Dame, US; ANU, Australia, Salzburg, Austria) for the analytical data during the last 30 years. We should thank also FAPERJ, CNPQ, CAPES and FINEP funding agencies, and joint projects with CPRM and Petrobras. This is contribution to IGCP 648.

References

Aguilar, C., Alkmim, F.F., Lana, C.C., Farina, F. 2017. Paleoproterozoic assembly of the São Francisco craton, SE Brazil: new insights from U–Pb titanite and monazite dating. Precambrian Research. 289, 95-115.

Alkmim F.F., Marshak S., Pedrosa-Soares A.C., Peres G.G., Cruz S.C.P., Whittington A. 2006. Kinematic evolution of the Araçuaí-West Congo orogeny in Brazil and Africa: Nutcracker tectonics during the Neoproterozoic assembly of Gondwana. Precambrian Research. 149, 43–64.

Alkmim F.F., Noce C.M. 2006. Outline of the geology of Quadrilátero Ferrífero. In: Alkmim F.F., Noce C.M. (Eds.), The Paleoproterozoic Record of São Francisco Craton. IGCP 509 Field Workshop, Bahia and Minas Gerais. Field Guide and Abstracts, 37–73.

Alkmim, F.F., Teixeira, W., 2017. The Paleoproterozoic Mineiro belt and the Quadrilátero Ferrífero. In: Heilbron M., Alkmim F., Cordani U.G. (Guest Ed.), The São Francisco Craton and its margins, Eastern Brazil. Regional Geology Review Series. Springer-Verlag, Chapter 5, 71–94.

Alkmim, F.F., Martins-Neto, M.A., 2012. Proterozoic first-order sedimentary sequences of the São Francisco craton, eastern Brazil. Marine and Petroleum Geology. 33, 127–139.

Alkmim, F.F., Marshak, S., Fonseca, M.A., 2001. Assembling West Gondwana in the Neoproterozoic: Clues from the São Francisco craton region, Brazil. Geology. 29, 319–322.

Almeida, F.F.M., Brito Neves, B.B., Carneiro, C.D.R., 2000. Origin and evolution of the South American Platform. Earth-Science Reviews. 50, 77–111.

Almeida, F.F.M.1981. O Cráton do Paramirim e suas relações com o do São Francisco. In: Simpósio Sobre o Cráton do São Francisco e Suas Faixas Marginais. Salvador. 1–10.

Ávila, C.A., Teixeira, W., Bongiolo, E.M., Dussin, I.A., 2014. The Tiradentes suite and its role in the Rhyacian evolution of the Mineiro belt, São Francisco Craton: Geochemical and U-Pb geochronological evidences. Precambrian Research. 243, 221–251.

Barbosa, J.F.S., Cruz S.P., Souza J.S. 2012. Terrenos metamórficos do embasamento. In: Barbosa JFS (Ed.), Geologia da Bahia: pesquisa e atualização, CBPM 1: 101–201.

Barbosa, J.S.F., Barbosa, R.G., 2017. The Paleoproterozoic Eastern Bahia Orogenic Domain. In: Heilbron M., Alkmim F., Cordani U.G. (Guest Ed.), The São Francisco Craton and its margins, Eastern Brazil. Regional Geology Review Series. Springer-Verlag, Chapter 4, 57-70.

Barbosa, J.S.F., Sabaté, P., 2004. Archean and Paleoproterozoic crust of the São Francisco Craton, Bahia, Brazil: geodynamic features. Precambrian Research, 133, 1–27.

Barbosa, N.S., Teixeira W., Ávila C.A., Montecinos P.M., Bongiolo E.M., 2015. 2.17–2.10 Ga plutonic episodes in the Mineiro belt, São Francisco Craton, Brazil: U-Pb ages, geochemical constraints and tectonics Precambrian Research. 270, 204-225

Barbosa, N.S., Teixeira W., Ávila C.A., Montecinos P.M., Bongiolo E.M. Vasconcelos, F.F., 2019. U-Pb geochronology and coupled Hf-Nd-Sr isotopic-chemical constraints of the Cassiterita Orthogneiss (2.47–2.41-Ga) in the Mineiro belt, São Francisco craton: Geodynamic fingerprints beyond the Archean-Paleoproterozoic Transition. Precambrian Research;326, 399-416.

Barbosa, O., 1954. Evolution du geossinclinal Espinhaço. In: International Geological Congress. *Comptes. Rendus*, section XIII, 19e session: 1-37.

Bédard, J., 2006. A catalytic delamination-driven model for coupled genesis of Archaean crust and sub-continental lithospheric mantle. Geochimica et Cosmochimica Acta 70, 1188–1214.

Bersan, S.M., Danderfer Filho A., Abreu F. R., Lana, C., 2018. Petrography, geochemistry and geochronology of the potassic granitoids of the Rio Itacambiruçu Supersuite: implications for the Meso- to Neoarchean evolution of the Itacambira-Monte Azul block. Brazilian Journal of Geology. 48(1), 1-24.

Boynton, W.V., 1984. Cosmochemistry of the rare earth elements: meteorite studies, In: P. Henderson (Ed.), Rare Earth Element Geochemistry (Developments in Geochemistry 2), Elsevier. 63-114

Brito-Neves, B.B., 2002. Main stages of development of sedimentary basins of South America and their relationships of tectonics of supercontinents. Gondwana Reserarch. 5, 175–196.

Brito-Neves, B.B., Campos Neto M.C., Fuck R., 1999. From Rodinia to Western Gondwana: An approach to the Brasiliano/Pan-African cycle and orogenic collage. Episodes. 22, 155–199

Brito-Neves, B.B., Sá J.M., Nilson, A.A., Botelho, N.F., 1996. A tafrogênese estateriana nos blocos paleoproterozóicos da América do Sul e processos subseqüentes. Geonomos. 3, 1–21.

Brueckner, H.K., Cunningham, D., Alkmin, F.F., Marshak, S., 2000. Tectonic implications of Precambrian Sm–Nd dates from the southern São Francisco craton and adjacent Araçuai and Ribeira belts, Brazil. Precambrian Research. 99 (3), 255–269.

Campos Neto, M.C., 2000. Orogenic Systems from Southwestern Gondwana: An approach to Brasiliano-Pan African Cycle and Orogenic Collage in Southeastern Brazil. In: Cordani, U.G.; Milani, E.J.; Thomaz Filho, A.; Campos, D.A. (eds.) Tectonic Evolution of South América. Rio de Janeiro, 31st International Geological Congress, Rio de Janeiro, p. 335–365.

Caro, G., Bourdon, B., 2010. Non-chondritic Sm/Nd ratio in the terrestrial planets: Consequences for the geochemical evolution of the mantle–crust system. Geochimica et Cosmochimica Acta. 74(11), 3333-3349.

Cawood, P. A., Hawkesworth, C. J., Pisarevski, S. A., Dhuime, B., Capitanio, F.A., Nebel, O., 2018. Geological archive of the onset of plate tectonics. Philosophical Transactions Royal Society A 376, 1-30.

Condie, K. C., 2005. TTGs and adakites: are they both slab melts? Lithos 80, 33–44.

Condie, K.C., Kröner, A., 2008. Special Paper of the Geological Society of America, 440, 281-294.

Cordani, U.G., Sato, K., 1999. Crustal evolution of the South American Platform based on Sm-Nd isotopic systematic on granitoid rocks. Episodes. 22, 167–173

Cox, K.G., Bell, J.D., Pankhurst, R.J., 1979. The Interpretation of Igneous Rocks. Allen & Unwin, London.

Cruz, S.C.P., Barbosa, J.S.F., Pinto, M.S., Peucat, J.-J., Paquette, J.L., Santos de Souza, J., de Souza Martins, V., Chemale Jr, F.., Carneiro, M.A., 2016. The Siderian-Orosirian magmatism in the Archean Gavião Paleoplate, Brazil: U–Pb geochronology, geochemistry and tectonic implications. Journal of South American Earth Sciences. 69, 43-79.

Cruz, S.C.P., Barbosa, J.S.F., Teixeira, L., Alkmim, F.F., Paquette, J. L., Peucat, J.J., 2015. O arco magmático sideriano-Riaciano (2,324–2,050 Ma) desenvolvido na margem continental Gavião, Bahia, Brasil. In: 15th Simpósio Naciaonal de Estudos Tectônicos, SNET. 205–208.

Cutts, K.A., Lana, C., Alkmim, F., Peres, G., 2018. Metamorphic imprints on units of the southern Araçuaí Belt, SE Brazil: the history of superimposed Transamazonian and Brasiliano orogenesis. Gondwana Research. 58, 211-234.

D'Agrella-Filho, M.S., Cordani, U.G., 2017. The Paleomagnetic Record of the São Francisco-Congo Craton. In: Heilbron M., Alkmim F., Cordani U.G. (Guest Ed.), The São Francisco Craton and its margins, Eastern Brazil. Regional Geology Review Series. Springer-Verlag, Chapter 17, 321–331.

De Paolo, D.J., 1981. Trace Element and Isotopic Effects of Combined Wallrock Assimilation and Fractional Crystallization. Earth and Planetary Science Letters, 53, 189-202.

Degler, R., Pedrosa-Soares, A., Novo, T., Tedeschi, M., Silva, L.C., Dussin, I., Lana, C., 2018. Rhyacian-Orosirian isotopic records from the basement of the Araçuaí-Ribeira orogenic system (SE Brazil): Links in the Congo-São Francisco palaeocontinent. Precambrian research. 317, 179-195.

Dhuime, B., Hawkesworth C.J., Cawood P.A., Storey C.D., 2012 A change in the geodynamics of continental growth 3 billion years ago. Science 335, 1334–1336.

Dhuime, B., Wuestefeld, A., Hawkesworth, C.J., 2015. Emergence of modern continental crust about 3 billion years ago. Nature Geoscience 8, 552–555

Duarte, B.P., Valente, S.C., Heilbron, M., Campos Neto, M.C., 2004. Petrogenesis of the orthogneisses of Mantiqueira Complex, central Ribeira belt, SE Brazil: An Archaean to Palaeoproterozoic basement unit reworked during the Pan-African Orogeny. Gondwana Research 7 (2), 437–450.

Farina, F., Albert, C., Martínez-Dopico, C., Aguilar Gil, C., Moreira, H., Hippertt, J.P., Cutts, K., Alkmim, F.F., Lana, C.. 2015. The Archean-Paleoproterozoic evolution of the Quadrilátero Ferrífero (Brasil): Current models and open questions. Journal of South American Earth Sciences. 68, 4–21.

Foley, S. F., Tiepolo, M., Vannucci, R., 2002. Growth of early continental crust controlled by melting of amphibolite in subduction zones. Nature 417, 637–40.

Fowler, M., Kocks, H., Darbyshire, D., Greenwood, P., 2008. Petrogenesis of high Ba-Sr granitoids from the Northern Highland Terrane of the British Caledonian Province. Lithos 105 (1-2), 129-148.

Fowler, M.B., Henney, P.J., Darbyshire, D.P.F., Greenwood, P.B., 2001. Petrogenesis of high Ba–Sr granites: the Rogart pluton, Sutherland. Journal of Geological Society of London 158, 521-534.

Frost, B.R., Barnes, C.G., Collins, W.J., Arculus, R.J., Ellis, D.J, Frost, C.D., 2001. A geochemical classification for granitic rocks. Journal of Petrology 42, 2033-2048.

Fuck, R., Brito-Neves, B.B., Schobbenhaus, C., 2008. Rodinia descendants in South America. Precambrian research. 160 (1), 108-126.

Gale, A., Dalton, C.A., Langmuir, C.H., Su, Y., Schilling, J.G., 2013. The mean composition of ocean ridge basalts. Geochemistry, Geophysics, Geosystems. 14(3), 489-518.

Goulart, L.E.A., Carneiro M.A., Endo I., Suita M.T.F., 2013. New evidence of Neoarchean crustal growth in southern São Francisco Craton: the Carmópolis de Minas Layered Suite, Minas Gerais, Brazil. Brazilian Journal of Geology. 43(3). 445–459

Halla, J., 2005. Late Archean high-Mg granitoids (sanukitoids) in the southern Karelian domain, eastern Finland: Pb and Nd isotopic constraints on crust-mantle interactions. Lithos 79 (1–2), 161–78.

Halla, J., van Hunen, J., Heilimo, E., Hölttä, P., 2009. Geochemical and numerical constraints on Neoarchaean plate tectonics. Precambrian Research 174, 155–162.

Haralyi, N.L.E., Hasui, Y., 1982. The gravimetric information and Archean-Proterozoic structural framework of eastern Brazil. Revista Brasileira de Geociências 112(1–3), 160–166.

Hastie, A., Fitton, J.G., Bromiley, G.D., Butler, I.B., Odling, N.W.A., 2016. The origin of Earth’s first continents and the onset of plate tectonics. Geology 44(10), 855-858.

Hasui, Y., Oliveira, M.A.F., 1984. A Província Mantiqueira: Setor Central. In: Almeida, F.F.M., Hasui, Y. (Eds.), O Precambriano do Brasil, Edgard Blucher, São Paulo, 308-344.

Hawkesworth, C. J., Cawood, P. A., Dhuime, B., 2016. Tectonics and crustal evolution. GSA Today 26(9), 4-11.

Hawkesworth, C., Cawood, P., Dhuime, B., 2013. Continental growth and the crustal record. Tectonophysics 609, 651–660

Hawkesworth, C.J., Dhuime, B., Pietranik, A., Cawood, P.A., Kemp, A. I. S., Storey, C.D., 2010. The generation and evolution of the continental crust. Journal of the Geological Society 167(2), 229-248

Heilbron, M., Duarte, B.P., Valeriano, C.M., Simonetti, A., Machado, N., Nogueira, J.R., 2010. Evolution of reworked Paleoproterozoic basement rocks within the Ribeira belt (Neoproterozoic), SE-Brazil, based on U-Pb geochronology: Implications for paleogeographic reconstructions of the São Francisco-Congo paleocontinent. Precambrian Research. 178, 136–148

Heilbron, M., Valeriano, C.M., Tassinari, C.C.G., Almeida, J.C.H., Tupinamba M, Siga, O., Trouw, R., 2008. Correlation of Neoproterozoic terranes between the Ribeira Belt, SE Brazil and its African counterpart: comparative tectonic evolution and open questions. Geological Society of London, Special Publication 294.

Heilbron, M. Ribeiro, A., Valeriano, C.M., Pacciullo, F.V., Almeida, J.C.H., Trouw, R. J., Tupinambá, M., Eirado Silva, L. G., 2017. The Ribeira Belt. In: Heilbron M., Alkmim F., Cordani U.G. (Guest Ed.), The São Francisco Craton and its margins, Eastern Brazil. Regional Geology Review Series. Springer-Verlag, Chapter 15, 277-302.

Heilbron, M., Duarte, B.P., Nogueira, J.R., 1998. The Juiz de Fora complex of the Central Ribeira belt, SE Brazil: a segment of Paleoproterozoic granulitic crust thrust during the Pan-African Orogen. Gondwana Research. 1(3), 373-381.

Heilbron, M., Pedrosa-Soares, A. C., Campos Neto, M. C., Silva, L. C., Trouw, R., Janasi, V. A., 2004. Brasiliano orogens in Southeast and South Brazil. Journal of the Virtual Explorer, 17

Heilimo, E., Halla, J., Huhma, H., 2011. Single-grain zircon U-Pb age constraints for the eastern and western sanukitoid zones in the Finnish Part of the Karelian Province. Lithos 121, 87–99.

Hiraga, R., Nogueira, J.R., Duarte, B.P., Valladares, C.S., Guimarães, V.O.M., Peterner, R., 2017. Geology and Lithogeochemistry of the Supracrustal Sequence and Interlayered metabasites of NE Santos Dumont Region (MG). Anuário do Instituto de Geociências 40(3), 359-376.

Irvine, T.M., Baragar, W.R., 1971. A guide to the chemical classification of common volcanic rocks. Canadian Journal of Earth Sciences 8, 523-548.

Kemp, A.I.S., Wilde, S.A., Hawkesworth, C.J., Coath, C.D., Nemchin, A., Pidgeon, R.T., Vervoort, J.D., DuFrane, S.A., 2010. Hadean crustal evolution revisited: New constraints from Pb-Hf isotope systematics of the Jack Hills zircons. Earth and Planetary Science Letters 296(1-2), 245–56,

Korenaga, J., 2013 Initiation and evolution of plate tectonics on earth: theories and observations. Ann. Rev. Earth Planet. Sci. 41, 117–151

Kovalenko, A., Clemens, J. D., Savatenkov, V., 2005. Petrogenetic constraints for the genesis of Archaean sanukitoid suites: geochemistry and isotopic evidence from Karelia, Baltic Shield. Lithos 79 (1–2), 147–60.

Kuribara, Y., Tsunogae, T., Santosh, M., Takamura, Y., Costa, A.G., Rosière, C.A., 2019. Eoarchean to Neoproterozoic crustal evolution of the Mantiqueira and the Juiz de Fora Complexes, SE Brazil: Petrology, geochemistry, zircon U-Pb geochronology and Lu-Hf isotopes. Precambrian Research 323, 82-101.

Lana, C., Alkmim, F.F., Armstrong, R., Scholz, R., Romano, R., Nalini Jr., H.A., 2013. The ancestry and magmatic evolution of Archaean TTG rocks of the Quadrilátero Ferrífero province, southeast Brazil. Precambrian Research 231, 157–173.

Laurent, O., Martin H., Moyen J.F., Doucelance, R., 2014 The diversity and evolution of late Archean granitoids: evidence for the onset of 'modern-style' plate tectonics between 3.0 and 2.5 Ga. Lithos 205, 208–235

Machado, N., Carneiro, M.A., 1992. U − Pb evidence of late Archean tectono-thermal activity in the southern São Francisco shield, Brazil. Canadian Journal of Earth Sciences. 29, 2341–2346.

Martin, H., 1986. Effect of steeper Archean geothermal gradient on geochemistry of subduction-zone magmas. Geology 14, 753–756.

Martin, H., 1987. Petrogenesis of Archaean trondhjemites, tonalites and granodiorites from eastern Finland: major and trace element geochemistry. Journal of Petrology 28 (5), 921–53

Martin, H., 1999. The adakitic magmas: modern analogues of Archaean granitoids. Lithos 46(3), 411–29.

Martin, H., Moyen, J.F., 2002. Secular changes in TTG composition as markers of the progressive cooling of the Earth. Geology 30 (4), 319– 322.

Martin, H., Moyen, J.F., Rapp, R., 2010. Sanukitoids and the Archaean-Proterozoic boundary. Transactions of the Royal Society of Edinburgh: Earth Sciences 100, 15–33.

Martin, H., Smithies, R. H., Rapp, R., Moyen, J.F., Champion, D., 2005. An overview of adakite, tonalite–trondhjemite–granodiorite (TTG), and sanukitoid: relationships and some implications for crustal evolution. Lithos 79 (1–2), 1–24.

McDonough, W.F., Sun, W., 1995. The composition of the Earth. Chemical Geology 120 (3-4), 223-253.

Moreira, H., Seixas, L., Storey, C., Fowler, M., Lasalle, S., Stevenson, R., Lana, C., 2018. Evolution of Siderian juvenile crust to rhyacian high Ba-Sr magmatism in the Mineiro belt, southern São Francisco craton. Geoscience Frontiers 9, 977-995

Moyen, J.F., Laurent, O., 2018. Archean tectonic systems? A view from igneous rocks. Lithos (302-303), 99-125.

Moyen, J.F., Martin, H., 2012. Forty years of TTG research. Lithos 148, 312–336.

Noce, C.M., Pedrosa-Soares, A.C., Silva, L.C., Armstrong, R., Piuzana, D. 2007. Evolution of polycyclic basement in the Araçuaí Orogen based on U-Pb SHRIMP data: implications for the Brazil-Africa links in the Paleoproterozoic time. Precambrian Research 159, 60–78.

O'Connor, J. T., 1965. A classification for Quartz-rich igneous rocks based on feldspar ratios. U.S. Geol. Survey Prof Paper 525-B: B79-B84

Oliveira, A.H., 2004. Evolução Tectônica de um fragmento do Cráton São Francisco Meridional com base em aspectos estruturais, geoquímicos (rocha total) e geocronológicos (Rb–Sr, Sm-Nd, Ar-Ar, U-Pb). PhD Thesis. Escola de Minas, Universidade Federal de Ouro Preto. 134 p.

Oliveira, E.P., McNaughton, N.J., Armstrong, R., 2010. Mesoarchaean to Palaeoproterozoic growth of the northern segment of the Itabuna Salvador Curaçá orogen, São Francisco craton, Brazil. Geological Society, London, Special Publications. 338, 263–286.

Pearce, J.A. 1982. Trace element characteristics of lavas from destructive plate boundaries. In: Thorpe, R. S. (Ed.), Andesites: Orogenic Andesites and Related Rocks. John Wiley & Sons, Chichester, pp 525-548.

Peccerillo, A., Taylor, S.R., 1976. Geochemistry of Eocene calc-alkaline volcanic rocks from the Kastamonu area, Northern Turkey. Contribution to Mineralogy and Petrology. 58, 63-81.

Peres, G.G., Alkmim, F.F., Jordt-Evangelista, H., 2004. The southern Araçuaí belt and the Dom Silvério Group: Geologic architecture and tectonic significance. Anais da Academia Brasileira de Ciências. 76, 771–790.

Pinese, J.P.P., Teixeira., Piccirillo, E.M., Quéméneur, J.J.G., Bellieni G., 1995. The Precambrian Lavras mafic dykes, southern São Francisco Craton, Brazil: preliminary geochemical and geochronological results. In: Baer, G., Heimann, A. (Eds.), Physics and Chemistry of Dykes, Rotterdam – Netherlands; 3rd Int Dyke Conf, pp. 205–219.

Pinheiro, M.A.P., Suita, M.T.F., Lesnov, F.P., Tedeschi, M., Silva, L.C., Medvedev, N.S., Korolyuk, V.N., Pinto, C.P., Sergeev, S.A., 2019. Timing and petrogenesis of metamafic-ultramafic rocks in the Southern Brasília orogen: Insights for a Rhyacian multi-system suprasubduction zone in the São Francisco paleocontinent (SE-Brazil). Precambrian research 321, 328-348.

Rajesh, H.M., Belyanin, G.A., Van Reenen, D.D., 2018. Three tier transition of Neoarchean TTG-sanukitoid magmatism in the Beit Bridge Complex, Southern Africa. Lithos 296-299, 431-451.

Rapp, R. P., Watson, E. B., 1995. Dehydration melting of metabasalt at 8–32 kbar: implications for continental growth and crust-mantle recycling. Journal of Petrology 36 (4), 891–931.

Rapp, R. P., Shimizu, N., Norman, M. D., 2003. Growth of early continental crust by partial melting of eclogite. Nature 425, 605–9.

Romano, R., Lana, C., Alkmim, F.F., Stevens, G., Armstrong, R., 2013. Stabilization of the southern portion of the São Francisco craton, SE Brazil, through a long-lived period of potassic magmatism. Precambrian Research 224, 143–159.

Sacanni, E., 2015. A new method of discriminating different types of post-Archean ophiolitic basalts and their tectonic significance using Th-Nb and Ce-Dy-Yb systematics. Geoscience Frontiers 6(4), 481-501.

Schobbenhaus, C., Brito Neves, B.B., 2003. Geology of Brazil in the context of the South American Platform. In: Bizzi, L.A., Schobbenhaus, C., Vidotti, R.M., Gonçalves, J.H. (Eds.), Geology, Tectonics and Mineral Resources of Brazil. Serviço Geológico – CPRM. 5–54

Shand, S. J., 1943. Eruptive rocks, 2nd ed. John Wiley, New York, pp 1-444.

Silva, L.C., Armstrong, R., Noce, C.M., Carneiro, M.A., Pimentel, M.M., Pedrosa-Soares, A.C., Leite, C.A., Vieira, V.S., Silva, M.A., Paes, V.J.C., Cardoso-Filho, J.M., 2002. Reavaliação da evolução geológica em terrenos pré-cambrianos brasileiros com base em novos dados U-Pb SHRIMP, parte II: Orógeno Araçuaí, Cinturão Mineiro e Cráton São Francisco Meridional. Revista Brasileira de Geociências. 32, 513–528.

Silva, L.C., Pedrosa-Soares, A.C., Armstrong, R., Pinto, C.P., Magalhães, J.T.R., Pinheiro, M.A.P., Santos, G.G., 2016. Disclosing the Paleoarchean to Ediacaran history of the São Francisco craton basement: The Porteirinha domain (northern Araçuaí orogen, Brazil). Journal of South American Earth Sciences 68, 50-67.

Sizova, E., Gerya, T., Brown, M., Perchuk, L.L., 2010. Subduction styles in the Precambrian: insight from numerical experiments. Lithos 116, 209–229.

Sun, W., McDonough, W.F., 1989. Chemichal and isotopic systematics of oceanic basalts: Implications for mantle composition and processes. Geological Society of London Special Publications. 42 (1), 313-345.

Tang, M., Chen, K., Rudnick, R.L., 2016 Archean upper crust transition from mafic to felsic marks the onset of plate tectonics. Science 351, 372–375.

Tarney, J., Jones, C.E., 1994. Trace element geochemistry of orogenic igneous rocks and crustal growth models. Geological Society of London Journal, 151, 855-868.

Teixeira, W., Figueiredo, M.C.H., 1991. An outline of Early Proterozoic crustal evolution in the Sao Francisco craton, Brazil: a review. Precambrian Research 53, 1-22.

Teixeira, W., Ávila, C.A., Dussin, I.A., Neto, A.C., Bongiolo, E.M., Santos, J.O., Barbosa, N.S., 2015. A juvenile accretion episode (2.35–2.32 Ga) in the Mineiro belt and its role to the Minas accretionary orogeny: Zircon U–Pb–Hf and geochemical evidences. Precambrian Research 256, 148–169.

Teixeira, W., Carneiro, M.A., Noce C.M., Machado, N., Sato, K., Taylor, P.N., 1996. Pb, Sr and Nd isotopic constraints on the Archean evolution of gneissic-granitoid complexes in the southern São Francisco Craton, Brazil. Precambrian Research 78, 151–164.

Teixeira, W., Oliveira, E.P., Marques, L.S., 2017. Nature and Evolution of the Archean Crust of the São Francisco Craton. In: Heilbron, M., Alkmim, F., Cordani, U.G. (Eds.), The São Francisco Craton and its margins, Eastern Brazil. Regional Geology Review Series. Springer-Verlag, Chapter 3, 29–55.

Teixeira, W., Sabaté, P., Barbosa J., Noce, C.M., Carneiro, M.A., 2000. Archean and Paleoproterozoic tectonic evolution of the São Francisco Craton. In: Cordani, U.G., Milani, E.J., Thomaz Fo, A., Campos, D.A. (Eds.), Tectonic Evolution of South América. Rio de Janeiro, 31st International Geological Congress, Rio de Janeiro. 101–137.

Trompette, R., 1994. Geology of Western Gondwana (2000–500 Ma): Pan-African-Brasiliano Aggregation of South America and Africa. Rotterdam, Balkema, 350 pp.

Trouw, R.A.J., Heilbron, M., Ribeiro, A., Paciullo, F.V.P., Valeriano, C.M., Almeida, J.C.H., Tupinambá, M., Andreis, R.R., 2000. The central segment of the Ribeira belt. In: Cordani, U.G., Milani, E.J., Thomaz Filho, A., Campos, D.A. (Eds.), Tectonic Evolution of South America, 31th International Geological Congress, Rio de Janeiro, Brazil, pp. 287–310

Whalen, J. B., Currie, K. L., Chappell, B. W., 1987. A-type granites: geochemical characteristics, discrimination and petrogenesis. Contribution to Mineralogy and Petrology 95, 407-419

Windley, B.F., Garde, A.A., 2009. Arc-generated blocks with crustal sections in the North Atlantic craton of West Greenland: Crustal growth in the Archean with modern analogues. Earth-Science Reviews 93, 1-30.

Figures Captions

Figure 1. Geological setting of the São Francisco Paleocontinent. (A) Gondwana configuration adapted from D'Agrella-Filho and Cordani (2017). (B) Archean blocks and Paleoproterozoic magmatic arcs of the São Francisco-Congo Paleocontinent. Modified from Alkmin and Teixeira, 2017; Barbosa and Barbosa, 2017; Degler et al., 2018.

Figure 2 Tectonic map of the study area within the reworked part of the southern São Francisco Paleocontinent in the Neoproterozoic (Modified from Peres et al., 2004; Alkmin and Teixeira, 2017). Compiled U-Pb data from (a) Heilbron et al., 2010; (b) Silva et al., 2002; (c) Pinheiro et al., 2019.

Figure 3 Field photographs of representative lithologies of the Mantiqueira Complex and Piedade Block. (A) Centimeter-scale compositional banding in orthogneiss with migmatitic textures. (B) Hornblende-bearing leucosomes surrounded by melanosomes rich in hornblende, biotite and plagioclase. (C) Megacrystic granodiorites displaying megacrysts of pale pink K-feldspar. (D, E). Dioritic hornblende biotite orthogneiss with migmatitic texture. (F) Metric layer of amphibolite showing sharp contact with the country rock (hornblende-biotite orthogneiss).

Figure 4. Photomicrographs from thin sections of the studied orthogneisses and metabasic rocks. (A) Sample 08: Hornblende-biotite orthogneiss. (B) Sample 09 under crossed nicols. (C) Sample 64B: Plagioclase and K-feldspar megacrystic hornblende-biotite orthogneiss. (D) Sample 64B under crossed nicols. (E) Sample 66A: Orthopyroxene Hornblende Biotite gneiss under granulite facies metamorphism. (F)

Sample 66A under crossed nicols. (G) Sample 103C: Amphibolite bearing hornblende, plagioclase, k-feldspar, biotite and titanite. (H) Sample 103C under crossed nicols. (I) Sample 21A: Amphibolite bearing clinopyroxene, hornblende, plagioclase, quartz, biotite and garnet. (J) Sample 19B bearing clinopyroxene, hornblende, plagioclase, quartz, biotite and garnet.

Figure 5 Cathodoluminescence (CL) and Backscattered electrons (BSE) images of representative grains of the Piedade Block (A–G). Circles indicate spot locations for U-Pb results. Zircon codes refer to analytical ID in U-Pb data table in Supplementary Material B. Data in pink colour is interpreted as inheritance, in red as crystallization and in blue as metamorphism. Paleoproterozoic and Archean data are shown in $^{207}Pb/^{206}Pb$ and Neoproterozoic data in $^{206}Pb/^{238}U$.

Figure 6. Concordia diagrams (A–G) presenting zircon U-Pb results for the rocks of the Piedade Block. Grey ellipses in the samples 21A (C), 21B (D), 19B (G) figures are interpreted as inherited zircons.

Figure 7. Cathodoluminescence (CL) and Backscattered electrons (BSE) images of representative grains of the Mantiqueira Complex (A–H). Circles indicate spot locations for U-Pb results. Zircon codes refer to analytical ID in U-Pb data table in Supplementary Material B. Data in pink colour is interpreted as inheritance, in red as crystallization and in blue as metamorphism. Paleoproterozoic and Archean data are shown in $^{207}Pb/^{206}Pb$ and Neoproterozoic data in $^{206}Pb/^{238}U$.

Figure 8. Concordia diagrams (A–G) presenting zircon U-Pb results for the rocks of the Mantiqueira Complex.

Figure 9. (A) AFM diagram of Irvine and Baragar (1971) showing the intermediate and acid samples plotting in the calc-alkaline series and the basic rocks in the tholeiite

series. (B) Triangular diagram Rb-Ba-Sr with the field for High Ba-Sr granites from Tarney and Jones (1994).

Figure 10. Geochemical classification of the studied granitoids. (A) TAS diagram (SiO_2 vs. Na_2O+K_2O) of Cox (1979) showing the WPT and WPA groups plotting in the basic, gabbro and subalkaline/tholeiitic series fields of the diagram, Group 1 plotting in the acid band of the diagram and in the granodiorite and granite fields, Group 2 plotting in the intermediate band in the diorite field, Group 3 straddling in the limit between the alkaline and subalkaline series and plotting in the intermediate and acid bands of the diagram, Sample 355 plotting in the syenite field of the alkaline series. (B) In the SiO_2 vs. K_2O diagram (Peccerillo and Taylor, 1976), samples of the Groups 1 and 2 plots in the medium-K calc-alkaline series whereas Group 3 plot in the high-K calc-alkaline series.

Figure 11. (A) $FeO^t/(FeO^t + MgO)$ vs. SiO_2 (Frost et al., 2001) diagram showing Groups 1 and 2 in the magnesian field and Group 3 straddling in the limit between magnesian and ferroan granitoid rocks. (B) In the $Na_2O + K_2O – CaO$ vs. SiO_2 (Frost et al., 2001) diagram samples from Group 1 plot in the calcic field, Group 2 straddles in the limit between calcic and calc-alkalic field and Group 3 plot mostly in the alkali-calcic field. (C) In the A/NK vs. A/CNK diagram (after Shand, 1943) samples from Group 1 are slightly peraluminous to metaluminous and samples from Group 2 and 3 are classified as metaluminous.

Figure 12. Left column (A – Group 1, C – Group 2, E – Group 3, G – Sample 355): Average chondrite-normalized REE patterns normalized after values from Boynton (1984); Right column (B – Group 1, D – Group 2, F – Group 3, H – Sample 355): Mantle-normalized multielement plots (McDonough and Sun, 1995).

Figure 13. Left column (A- WPA and C - WPT): Average chondrite-normalized REE patterns normalized after values from Boynton (1984); Right column (B – WPA and D – WPT): Mantle-normalized multielement plots (McDonough and Sun, 1995).

Figure 14. Nd evolution vs. time (crystallization ages) diagram. Samples from the Piedade Block are shown in open symbols and from the Mantiqueira Complex in filled symbols. The isotopic field of the Archean São Francisco Paleocontinent (grey) is compiled from Teixeira et al. (1996).

Figure 15. (A) Diagram for adakite/TTG discrimination (Martin, 1986). (B) Classification diagram for siliceous igneous rocks, based on feldspar composition (O'Connor, 1965). (C) Ternary classification diagram from Laurent et al. (2014). Vertices are: 2 × A/CNK (molar Al_2O_3/(CaO + K_2O + Na_2O) ratio); Na_2O/K_2O and 2 × (FeO^t + MgO) × (Sr + Ba) wt.% (=FMSB). (D) Ternary diagram Al_2O_3/ (FeO^t + MgO); 3 × CaO; 5 × (K_2O/Na_2O) proposed for Laurent et al. (2014) showing the composition of melts derived from a potential source.

Figure 16. Isotopic diagram for the Mantiqueira Complex and Piedade Block samples. (A) Sr evolution diagram (initial $^{87}Sr/^{86}Sr$ vs. Time (Ma)) of Ben Othman et al. (1984). Pink polygon represents the evolution of the Piedade block samples. (B) $^{143}Nd/^{144}Nd$ vs. $^{87}Sr/^{86}Sr$ diagram at the crystallization age of the samples. Mantle components (MORB) composition by Gale et al. (2013). (C) ε_{Nd} vs. initial $^{87}Sr/^{86}Sr$ diagram (Sr and Nd isotopic systematics of the crust and mantle, horizontal grey band is the estimated εNd of the bulk silicate of Caro and Bourdon (2010); vertical grey band between dashed lines in their estimated bulk silicate Earth $^{87}Sr/^{86}Sr$.

Figure 17. Variation in the thickness of new continental crust through time (red curve) diagram (Korenaga et al., 2013; Dhuime et al., 2015; Hawksworth et al., 2016) showing

two bands of TTG-sanukitoide suite generation (i.e. Neoarchean (Piedade block) and Rhyacian (Mantiqueira Complex).

Figure 18. Simplified age distribution for TTG, Sanukitoid, Hybrid and Biotite-Two-mica granitoid rocks in cratons around the world, including the Neoarchean and Rhyacian São Francisco Paleocontinent. (Modified after Heilimo et al., 2011; Laurent et al., 2014; Cawood et al., 2018). Data from São Francisco Paleocontinent from this study; Alkmim and Teixeira, 2017; Teixeira et al., 2017; Barbosa and Barbosa, 2017.

Figure 19. Integrated tectonic evolution model for the Mantiqueira Complex, southeast Brazil, as envisaged for the period between ca. 2.2 and 1.9 Ga (modified after Heilbron et al., 2010).

Figure 20. ε_{Nd} vs. ε_{Sr} diagram with distinct fields characterized by data from the Itabuna-Salvador-Curaçá Belt, Gavião, Serrinha and Jequié block (modified after Barbosa and Barbosa, 2017) and data from the Mantiqueira Complex and Piedade Block (from this study).

Tables Captions

Table 1 Summary of geochronological results of the Piedade Block and the Mantiqueira Complex. * Three discordia upper intercepts interpreted as inheritance: 3083 ± 20 Ma, 2617 ± 20 Ma, 2096 ± 33 Ma.

Table 2 Chemical analyses of major (wt.%), and trace elements (ppm) for samples of the Group 1.

Table 3 Chemical analyses of major (wt.%), and trace elements (ppm) for samples of the Group 2.

Table 4 Chemical analyses of major (wt.%), and trace elements (ppm) for samples of the Group 3 and Sample 355.

Table 5 Chemical analyses of major (wt.%), and trace elements (ppm) for the basic rocks of Group 1 (Samples 103C, 339C, 149, 21A) and Group 2 (70D, 141, 378, 66B and 19B).

Table 6 Sm-Nd and Sr whole rock analytical data for the Mantiqueira Complex and Piedade block samples.

Sample	Rock type	Crystallization age (Ma)	Inheritance age (Ma)	Metamorphism age (Ma)
Piedade Block				
66A	Felsic granulite	2693 ± 23	-	2043 ± 30
66B	Basic granulite	2710 ± 32	-	2067 ± 82
21A	Basic granulite	2523 ± 28	2690 ± 7	-
21B	Felsic granulite	2731 ± 24	3045 ± 26	2039 ± 16
148	Felsic granulite	2659 ± 23	-	2085 ± 38
19A	Felsic granulite	2715 ± 11	-	592 ± 26
19B	Basic granulite	1966 ± 7.9	*	-
Mantiqueira Complex				
8	Hbl Bt gneiss	2168 ± 22	-	579 ± 5
67	Bt gneiss	2117 ± 28	-	553 ± 75
163A	Opx Hbl Bt gneiss	2116 ± 15	-	561 ± 12
137G	Hbl Bt gneiss	2023 ± 13	-	535 ± 28
64A	Hbl Bt gneiss	2106 ± 27	-	563 ± 24
64B	Hbl Bt gneiss	2107 ± 17	-	567 ± 41
103C	Amphibolite	2044 ± 6	-	661 ± 64
355	Hbl Bt gneiss	1983 ± 13	-	557 ± 14
70D	Amphibolite	1989 ± 13	-	610 ± 33

Sample	163F	163A	12A	109A	50	67	19A
SiO_2	62.9	63.6	66.2	71.3	71.8	72.3	62.2
Al_2O_3	16.8	17.2	15.6	14.9	14.7	15.5	16.7
FeO^t	5.1	4.3	4.8	2.6	2.3	1.5	6.2
$Fe_2O_3^t$	5.7	4.7	5.3	2.9	2.5	1.7	6.9
MnO	0.1	0.1	0.1	0.0	0.0	0.0	0.1
MgO	1.7	1.4	1.8	0.9	0.8	0.5	3.0
CaO	4.8	5.1	3.6	3.4	2.3	3.2	5.8
Na2O	4.3	4.5	3.8	4.4	4.4	4.6	3.3
K2O	1.4	1.2	2.5	1.9	2.5	2.0	1.3
TiO2	0.5	0.5	0.4	0.4	0.4	0.3	0.7
P2O5	0.2	0.2	0.1	0.1	0.1	0.1	0.3
LOI	0.4	0.3	0.8	0.4	0.4	0.4	0.4
Total	98.7	98.7	100.2	100.7	99.8	100.5	100.8
Na_2O/K_2O	3.1	3.8	1.6	2.3	1.7	2.3	2.527
Mg# ×100	44.0	34.0	39.9	43.0	37.2	37.0	46.470
Sc	9.0	4.0	8.0	2.0	3.0	2.0	15.0
Be	2.0	3.0	2.0	3.0	1.0	2.0	2.0
V	58.0	47.0	77.0	36.0	19.0	13.0	139.0
Ba	459.0	416.0	563.0	725.0	1365.0	1477.0	519.0
Sr	596.0	636.0	326.0	557.0	459.0	837.0	362.0
Y	9.0	7.0	10.0	17.0	6.0	4.0	11.0
Zr	151.0	204.0	125.0	128.0	199.0	118.0	274.0
Cr	< 20	< 20	40.0	60.0	< 20	< 20	30.0
Co	9.0	7.0	11.0	12.0	13.0	19.0	29.0
Ni	< 20	< 20	< 20	< 20	< 20	< 20	30.0
Cu	< 10	< 10	30.0	< 10	< 10	30.0	60.0
Zn	60.0	50.0	50.0	40.0	50.0	< 30	90.0
Ga	19.0	21.0	19.0	19.0	19.0	18.0	21.0
Ge	< 1	< 1	1.0	< 1	< 1	< 1	1.0
As	< 5	< 5	< 5	< 5	< 5	< 5	< 5
Rb	33.0	25.0	115.0	52.0	39.0	40.0	40.0
Nb	3.0	5.0	4.0	4.0	3.0	2.0	8.0
Mo	< 2	< 2	< 2	< 2	< 2	< 2	< 2
Ag	< 0.5	< 0.5	< 0.5	< 0.5	0.6	< 0.5	< 0.5
In	< 0.2	< 0.2	< 0.2	< 0.2	< 0.2	< 0.2	< 0.2
Sn	1.0	< 1	< 1	1.0	< 1	< 1	< 1
Sb	< 0.5	< 0.5	< 0.5	< 0.5	< 0.5	< 0.5	< 0.5
Cs	< 0.5	< 0.5	1.4	< 0.5	< 0.5	0.8	< 0.5
La	17.4	34.2	21.4	24.1	78.7	15.7	29.1
Ce	32.9	59.8	37.4	35.6	130.0	29.0	54.2
Pr	3.7	5.9	3.9	3.7	12.9	3.2	6.1
Nd	14.2	19.6	13.0	12.2	42.2	12.3	22.3
Sm	2.7	3.0	2.3	1.7	5.6	2.1	3.8
Eu	1.2	1.3	0.9	0.9	1.8	1.0	1.5
Gd	2.3	2.0	2.0	1.7	3.4	1.4	3.1

Tb	0.3	0.2	0.3	0.2	0.4	0.2	0.4
Dy	1.7	1.2	1.6	1.2	1.5	0.9	2.2
Ho	0.3	0.2	0.3	0.3	0.3	0.1	0.4
Er	0.9	0.6	0.9	0.6	0.7	0.4	1.1
Tm	0.1	0.1	0.1	0.1	0.1	< 0.05	0.2
Yb	0.8	0.6	0.8	0.3	0.5	0.3	1.0
Lu	0.1	0.1	0.1	0.0	0.1	0.1	0.2
Hf	3.3	4.7	2.6	3.2	4.7	2.5	5.9
Ta	0.2	0.3	0.4	0.3	0.2	0.3	0.4
W	< 1	< 1	< 1	79.0	111.0	214.0	125.0
Tl	0.2	0.1	0.7	< 0.1	0.3	0.2	< 0.1
Pb	14.0	16.0	11.0	16.0	14.0	14.0	8.0
Bi	< 0.4	< 0.4	< 0.4	< 0.4	< 0.4	< 0.4	< 0.4
Th	0.6	0.8	2.6	0.4	13.3	2.5	0.4
U	0.3	0.7	0.6	0.4	0.3	0.8	0.4

Sample	148	21B	66A	134A	103A	103B	8	91B
SiO_2	58.1	57.9	59.3	56.4	58.2	59.5	57.1	61.8
Al_2O_3	15.8	15.3	15.3	17.4	18.3	17.1	18.0	16.2
FeO^t	8.5	8.1	6.9	7.0	7.0	6.8	6.1	5.9
$Fe_2O_3^t$	9.5	9.0	7.7	7.8	7.7	7.6	6.8	6.5
MnO	0.1	0.1	0.1	0.1	0.1	0.1	0.1	0.1
MgO	2.8	3.1	3.7	2.9	3.1	3.1	3.1	3.3
CaO	6.5	6.5	6.4	8.2	5.5	5.3	6.0	5.0
Na_2O	3.6	4.3	3.7	3.6	4.4	4.3	5.6	4.0
K_2O	1.1	1.6	1.8	1.5	1.9	1.8	1.4	1.9
TiO_2	1.5	1.4	1.0	1.1	1.0	0.9	0.9	0.7
P_2O_5	0.5	0.5	0.6	0.2	0.4	0.3	0.3	0.2
LOI	-0.2	0.4	1.1	0.8	0.4	0.6	0.5	0.6
Total	99.4	100.0	100.6	100.1	101.0	100.5	99.7	100.4
Na_2O/K_2O	3.2	2.6	2.0	2.4	2.3	2.4	4.1	2.1
Mg#×100	37.0	40.4	48.4	41.9	44.1	44.8	47.4	50.1
Sc	19.0	18.0	16.0	16.0	13.0	12.0	21.0	19.0
Be	2.0	2.0	2.0	3.0	2.0	2.0	3.0	2.0
V	175.0	158.0	130.0	159.0	121.0	122.0	125.0	103.0
Ba	572.0	892.0	544.0	607.0	1039.0	958.0	484.0	656.0
Sr	288.0	327.0	379.0	704.0	567.0	548.0	946.0	613.0
Y	41.0	51.0	29.0	28.0	16.0	15.0	43.0	15.0
Zr	524.0	481.0	263.0	249.0	195.0	249.0	224.0	176.0
Cr	30.0	40.0	80.0	60.0	60.0	60.0	30.0	90.0
Co	27.0	30.0	30.0	22.0	23.0	24.0	18.0	19.0
Ni	30.0	40.0	40.0	30.0	30.0	40.0	40.0	20.0
Cu	40.0	40.0	40.0	20.0	20.0	40.0	20.0	10.0
Zn	100.0	110.0	90.0	70.0	100.0	110.0	80.0	90.0
Ga	22.0	22.0	20.0	27.0	25.0	25.0	20.0	21.0
Ge	1.0	1.0	1.0	2.0	< 1	1.0	1.0	1.0
As	< 5	< 5	< 5	< 5	< 5	< 5	< 5	< 5
Rb	8.0	18.0	38.0	41.0	45.0	37.0	26.0	80.0
Nb	26.0	26.0	10.0	11.0	8.0	7.0	8.0	8.0
Mo	2.0	< 2	< 2	< 2	< 2	< 2	< 2	< 2
Ag	1.4	< 0.5	0.6	0.5	< 0.5	< 0.5	0.7	< 0.5
In	< 0.2	< 0.2	< 0.2	< 0.2	< 0.2	< 0.2	< 0.2	< 0.2
Sn	1.0	1.0	3.0	2.0	3.0	2.0	3.0	1.0
Sb	< 0.5	< 0.5	< 0.5	< 0.5	< 0.5	< 0.5	< 0.5	< 0.5
Cs	< 0.5	< 0.5	< 0.5	< 0.5	< 0.5	< 0.5	< 0.5	1.3
La	54.1	101.0	65.3	60.3	63.8	51.5	51.1	59.5
Ce	117.0	204.0	128.0	108.0	127.0	99.6	97.8	114.0
Pr	13.9	23.7	14.6	12.4	14.2	11.7	12.2	12.9
Nd	54.1	82.2	55.2	44.5	49.9	42.2	49.9	48.2
Sm	11.1	14.9	10.2	8.1	8.4	7.2	11.2	8.5
Eu	2.4	3.1	2.4	2.0	1.6	1.6	3.0	1.4
Gd	9.7	12.8	7.6	6.5	5.8	5.4	9.9	5.3

Tb	1.5	1.9	1.1	1.0	0.7	0.7	1.4	0.7
Dy	8.8	10.8	5.9	5.5	3.7	3.4	8.1	3.6
Ho	1.6	2.1	1.1	1.0	0.6	0.6	1.6	0.6
Er	4.4	5.7	3.2	2.8	1.6	1.5	4.2	1.6
Tm	0.6	0.8	0.4	0.4	0.2	0.2	0.6	0.2
Yb	3.8	5.0	2.7	2.8	1.2	1.2	3.6	1.2
Lu	0.6	0.8	0.4	0.4	0.2	0.2	0.5	0.2
Hf	10.6	10.2	5.5	5.7	4.4	5.3	5.0	3.8
Ta	1.7	1.1	0.8	0.8	0.3	0.2	0.4	0.3
W	47.0	56.0	85.0	37.0	56.0	36.0	55.0	48.0
Tl	< 0.1	< 0.1	0.2	< 0.1	< 0.1	< 0.1	0.2	0.5
Pb	12.0	9.0	9.0	17.0	13.0	12.0	16.0	9.0
Bi	< 0.4	< 0.4	< 0.4	< 0.4	< 0.4	< 0.4	< 0.4	< 0.4
Th	0.6	4.1	13.9	10.4	7.5	3.2	3.8	5.9
U	0.7	0.7	0.6	2.9	0.3	0.2	0.3	0.5

Sample	137F	137G	64A	64B	355*
SiO_2	58.0	53.5	65.2	53.8	56.2
Al_2O_3	15.9	15.8	14.3	17.2	12.8
FeO^t	8.2	10.5	5.1	8.5	6.8
$Fe_2O_3^t$	9.2	11.7	5.7	9.4	7.5
MnO	0.1	0.2	0.1	0.2	0.1
MgO	2.4	2.9	1.8	3.2	4.4
CaO	5.7	5.7	4.2	6.2	5.4
Na_2O	4.1	3.9	3.6	4.0	2.5
K_2O	2.6	2.8	2.7	2.4	7.4
TiO_2	1.7	2.0	1.0	1.6	1.3
P_2O_5	0.7	0.8	0.7	1.2	0.9
LOI	0.2	0.3	0.7	1.0	0.5
Total	100.4	99.4	99.8	100.2	98.9
Na_2O/K_2O	1.6	1.4	1.3	1.6	0.3
Mg#×100	34.2	32.7	38.1	40.3	53.6
Sc	18.0	23.0	12.0	22.0	17.0
Be	2.0	2.0	2.0	3.0	3.0
V	129.0	165.0	82.0	150.0	125.0
Ba	1758.0	1927.0	973.0	673.0	3981.0
Sr	607.0	530.0	526.0	525.0	1350.0
Y	42.0	50.0	44.0	59.0	32.0
Zr	526.0	622.0	306.0	429.0	317.0
Cr	< 20	40.0	< 20	40.0	160.0
Co	28.0	32.0	13.0	23.0	21.0
Ni	< 20	< 20	< 20	< 20	60.0
Cu	< 10	20.0	20.0	30.0	30.0
Zn	130.0	170.0	70.0	120.0	60.0
Ga	24.0	25.0	21.0	28.0	19.0
Ge	1.0	2.0	1.0	2.0	2.0
As	< 5	< 5	< 5	< 5	< 5
Rb	42.0	49.0	76.0	104.0	247.0
Nb	18.0	23.0	10.0	26.0	23.0
Mo	< 2	2.0	< 2	< 2	< 2
Ag	1.0	1.3	0.8	1.1	0.7
In	< 0.2	< 0.2	< 0.2	< 0.2	< 0.2
Sn	1.0	2.0	4.0	7.0	1.0
Sb	< 0.5	< 0.5	< 0.5	< 0.5	< 0.5
Cs	< 0.5	< 0.5	< 0.5	0.7	1.8
La	96.5	97.1	94.8	111.0	134.0
Ce	212.0	222.0	200.0	231.0	285.0
Pr	25.4	27.3	23.7	27.5	33.9
Nd	99.7	109.0	90.4	106.0	128.0
Sm	17.9	20.7	17.0	20.3	22.6
Eu	4.0	4.7	2.9	4.1	5.3
Gd	12.9	15.3	12.3	15.2	14.3

Tb	1.7	2.0	1.7	2.2	1.6
Dy	8.9	10.8	9.4	11.8	7.3
Ho	1.6	2.0	1.7	2.2	1.2
Er	4.2	5.1	4.4	5.8	2.9
Tm	0.5	0.7	0.6	0.8	0.3
Yb	3.4	4.3	3.6	5.1	2.0
Lu	0.5	0.7	0.5	0.8	0.3
Hf	10.9	13.5	6.0	9.1	6.1
Ta	0.9	1.1	0.7	1.9	1.4
W	122.0	90.0	54.0	53.0	< 1
Tl	< 0.1	< 0.1	0.3	0.5	0.9
Pb	13.0	14.0	15.0	16.0	15.0
Bi	< 0.4	< 0.4	< 0.4	< 0.4	< 0.4
Th	1.7	2.9	9.3	18.3	3.5
U	0.4	0.4	0.8	6.6	0.7

Sample	103C	339C	149	21A	141	378B	66B	19B	70D
SiO_2	46.1	47.3	49.7	48.8	49.4	52.2	47.5	52.1	48.3
Al_2O_3	13.9	13.8	12.5	16.1	13.4	12.2	14.2	14.5	12.9
FeO^t	13.0	12.7	14.9	12.7	14.6	10.8	14.4	11.0	14.6
$Fe_2O_3{}^t$	14.4	14.1	16.5	14.2	16.2	12.0	16.0	12.2	16.2
MnO	0.2	0.2	0.2	0.2	0.2	0.2	0.2	0.2	0.3
MgO	6.4	6.0	4.9	4.9	5.8	8.2	6.6	6.5	5.7
CaO	10.2	8.8	9.3	8.8	9.6	9.9	9.7	10.5	10.7
Na_2O	2.6	3.2	2.4	3.2	3.2	2.6	1.3	2.3	2.4
K_2O	1.0	0.8	0.8	0.6	1.0	1.2	0.7	0.8	1.2
TiO_2	3.2	3.3	3.4	2.2	1.3	0.9	1.5	0.9	2.4
P_2O_5	0.4	0.5	0.4	1.0	0.1	0.2	0.1	0.1	0.2
LOI	0.7	0.9	0.4	0.7	0.3	0.1	3.1	0.5	0.2
Total	99.2	98.9	100.5	100.6	100.6	99.6	100.8	100.6	100.5
Na_2O/K_2O	2.8	3.8	3.0	5.1	3.1	2.2	1.8	2.756	2.1
Mg#×100	46.9	45.8	37.2	40.5	41.6	57.5	44.8	51.130	41.1
Sc	37.0	31.0	41.0	26.0	45.0	37.0	49.0	41.0	50.0
Be	2.0	2.0	2.0	2.0	1.0	1.0	< 1	2.0	1.0
V	362.0	356.0	425.0	257.0	356.0	259.0	354.0	293.0	499.0
Ba	160.0	290.0	2736.0	401.0	271.0	1001.0	80.0	155.0	376.0
Sr	283.0	480.0	247.0	647.0	172.0	265.0	37.0	159.0	220.0
Y	33.0	26.0	50.0	35.0	26.0	18.0	22.0	24.0	28.0
Zr	273.0	224.0	242.0	353.0	78.0	75.0	106.0	60.0	124.0
Cr	50.0	70.0	60.0	100.0	60.0	350.0	90.0	210.0	90.0
Co	46.0	43.0	57.0	41.0	61.0	43.0	58.0	51.0	40.0
Ni	50.0	20.0	50.0	80.0	70.0	100.0	50.0	110.0	30.0
Cu	40.0	40.0	270.0	60.0	50.0	100.0	60.0	30.0	20.0
Zn	150.0	90.0	200.0	130.0	130.0	90.0	110.0	100.0	160.0
Ga	26.0	21.0	22.0	21.0	18.0	15.0	18.0	16.0	21.0
Ge	2.0	1.0	2.0	1.0	2.0	1.0	2.0	2.0	2.0
As	< 5	< 5	< 5	< 5	< 5	< 5	< 5	< 5	< 5
Rb	2.0	10.0	22.0	3.0	5.0	36.0	4.0	13.0	8.0
Nb	30.0	29.0	27.0	19.0	6.0	2.0	6.0	4.0	8.0
Mo	< 2	< 2	< 2	< 2	< 2	< 2	< 2	< 2	< 2
Ag	< 0.5	0.5	0.6	< 0.5	< 0.5	< 0.5	< 0.5	< 0.5	< 0.5
In	< 0.2	< 0.2	< 0.2	< 0.2	< 0.2	< 0.2	< 0.2	< 0.2	0.2
Sn	3.0	1.0	2.0	1.0	1.0	< 1	1.0	2.0	2.0
Sb	< 0.5	< 0.5	< 0.5	< 0.5	< 0.5	< 0.5	< 0.5	< 0.5	< 0.5
Cs	< 0.5	< 0.5	< 0.5	< 0.5	< 0.5	< 0.5	< 0.5	< 0.5	< 0.5
La	34.5	34.1	33.6	77.1	16.3	13.7	10.6	10.3	10.1
Ce	75.8	75.9	59.7	162.0	29.3	33.4	20.7	22.8	23.2
Pr	9.4	9.5	8.0	19.2	3.9	4.5	3.2	3.0	3.3
Nd	35.8	38.5	34.2	70.2	16.5	19.8	14.8	11.7	14.7
Sm	7.9	8.2	9.1	11.6	4.2	4.7	4.0	3.1	4.4
Eu	2.6	2.9	2.6	3.0	1.3	1.4	1.3	0.9	1.5
Gd	7.6	7.7	9.9	9.6	4.9	4.6	4.2	3.9	5.7

Tb	1.2	1.2	1.6	1.4	0.8	0.7	0.7	0.7	0.9
Dy	6.9	6.3	9.9	7.6	5.3	4.2	4.9	4.5	5.9
Ho	1.4	1.2	2.1	1.5	1.1	0.8	1.0	0.9	1.2
Er	3.9	3.1	5.8	4.0	3.2	2.3	2.8	2.7	3.5
Tm	0.5	0.4	0.8	0.5	0.5	0.3	0.4	0.4	0.5
Yb	3.5	2.5	5.2	3.3	3.0	2.1	2.9	2.5	3.3
Lu	0.5	0.4	0.8	0.5	0.5	0.3	0.4	0.4	0.5
Hf	6.1	4.5	6.2	6.2	2.3	1.8	2.4	1.4	3.2
Ta	2.0	2.1	1.9	1.1	0.4	0.2	0.4	0.4	0.5
W	24.0	< 1	90.0	20.0	30.0	< 1	11.0	59.0	25.0
Tl	< 0.1	< 0.1	< 0.1	< 0.1	< 0.1	0.2	< 0.1	< 0.1	< 0.1
Pb	9.0	15.0	< 5	7.0	8.0	< 5	5.0	6.0	10.0
Bi	< 0.4	< 0.4	< 0.4	< 0.4	< 0.4	< 0.4	< 0.4	< 0.4	< 0.4
Th	3.3	1.8	3.7	1.7	0.2	0.5	0.9	0.5	0.7
U	1.2	0.5	0.9	0.4	< 0.1	0.1	0.2	0.5	0.4

Sample	**70D**	**355**	**163A**	**137G**	**8**	**64A**	**64B**	**67**	**21A**	**148**	**21B**	**66A**
Sm (ppm)	4.8	22.6	3	21.2	11.4	15.8	21	1.9	12.6	10.8	14.9	10.1
Nd (ppm)	16.1	132.1	20.8	117.5	52.2	86.8	113.6	11.7	76.2	57.1	83.7	56.7
Crystallization (Ga)	1989	1983	2116	2023	2168	2106	2107	2100	2523	2659	2731	2693
$^{143}Nd/^{144}Nd$	0.512508	0.511195	0.510874	0.511171	0.511221	0.51132	0.511282	0.511271	0.510754	0.511005	0.510909	0.510883
abs. St. Error.	0.000005	0.000004	0.000006	0.000008	0.000005	0.000005	0.000004	0.000009	0.000006	0.000004	0.000005	0.000005
$^{147}Sm/^{144}Nd$	0.180003	0.1034	0.0862	0.109055	0.1317	0.1097	0.1118	0.0983	0.100079	0.1149	0.1075	0.1079
$^{87}Sr/^{86}Sr$ (m)	0.706182	0.721346	0.708256	0.711606	0.709437	0.71913	0.71937	0.70897	0.703626	0.70848	0.70973	0.718211
abs. St. Error.	0.000008	0.000006	0.000007	0.000007	0.000008	0.000005	0.000004	0.00001	0.000007	0.000009	0.000004	0.000005
$\varepsilon_{Nd}(t)$	1.7	-4.4	-4.7	-5.9	-9.7	-2.3	-3.5	-0.1	-5.4	-3.7	-2.5	-3.4
$^{143}Nd/^{144}Nd$ (i)	0.5102	0.5098	0.5097	0.5097	0.5093	0.5098	0.5097	0.5099	0.5091	0.5090	0.5090	0.5090
T_{DM} (Ga)	2.24	2.46	2.53	2.62	3.18	2.44	2.53	2.27	2.93	2.97	2.92	2.96
$^{87}Sr/^{86}Sr$ (i)	0.7032	0.7062	0.7048	0.7038	0.7069	0.7064	0.7019	0.7048	0.7031	0.7054	0.7034	0.7069

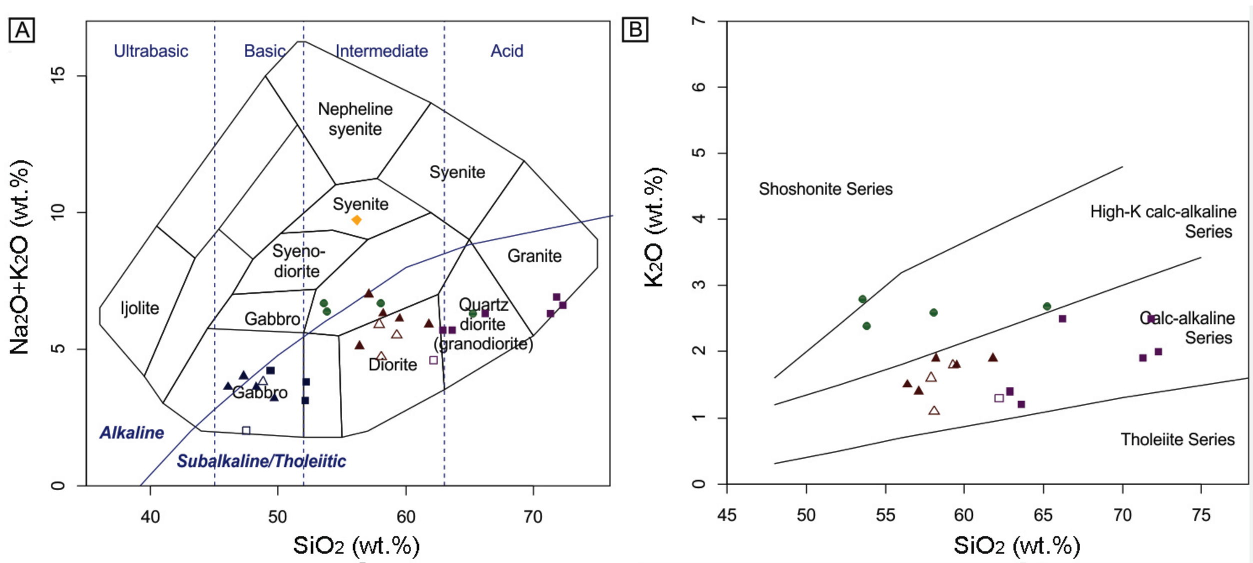
A
Ultrabasic
Basic
Intermediate
Acid
Nepheline syenite
Syenite
Syenite
Syeno-diorite
Ijolite
Gabbro
Granite
Quartz diorite (granodiorite)
Diorite
Gabbro
Alkaline
Subalkaline/Tholeiitic
Na2O+K2O (wt.%)
SiO2 (wt.%)
B
Shoshonite Series
High-K calc-alkaline Series
Calc-alkaline Series
Tholeiite Series
K2O (wt.%)
SiO2 (wt.%)

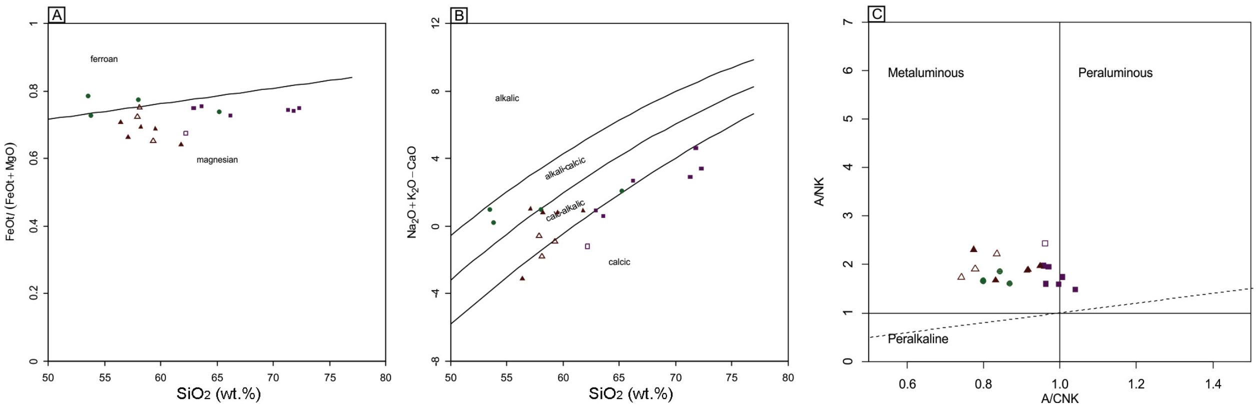
A
ferroan
magnesian
FeOt/ (FeOt+MgO)
SiO2 (wt.%)
B
alkalic
alkali-calcic
calc-alkalic
calcic
Na2O+K2O−CaO
SiO2 (wt.%)
C
Metaluminous
Peraluminous
Peralkaline
A/NK
A/CNK

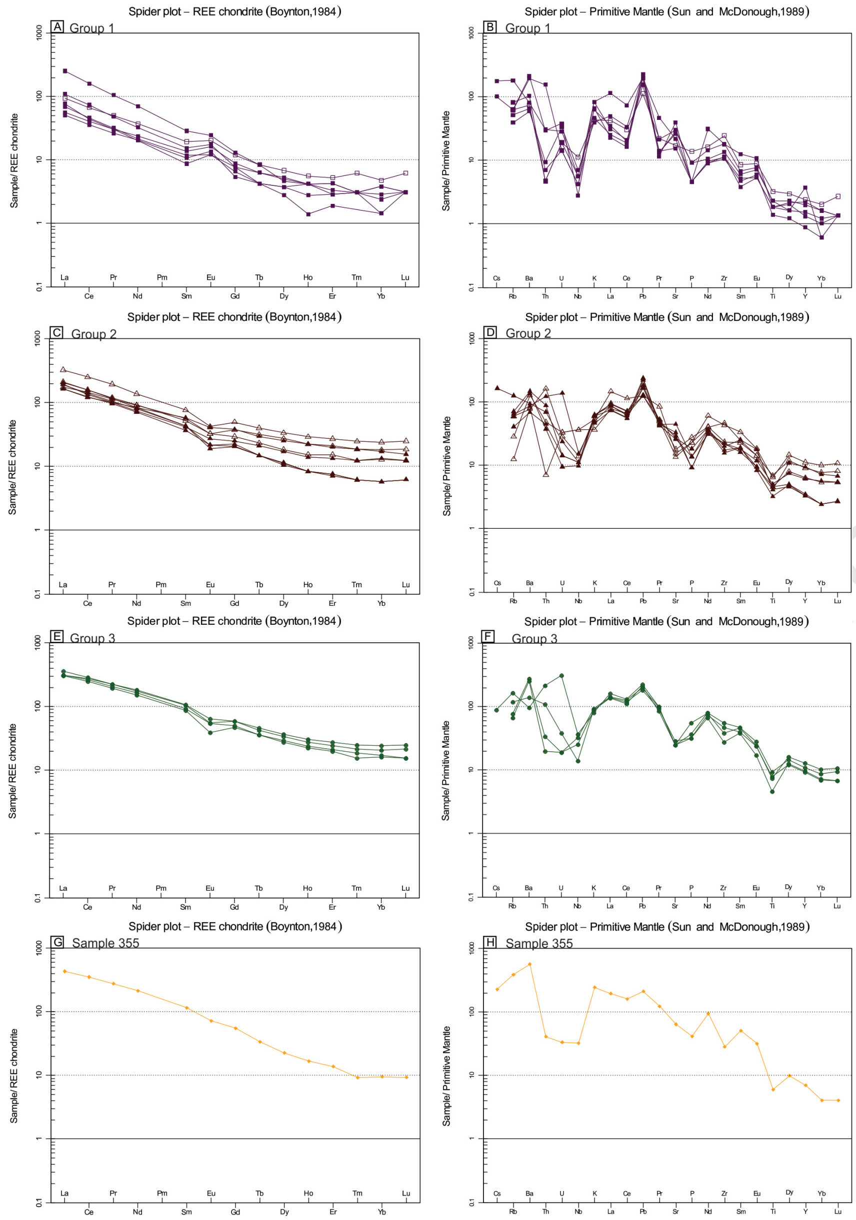
Spider plot – REE chondrite (Boynton,1984)
A Group 1
Spider plot – Primitive Mantle (Sun and McDonough,1989)
B Group 1
Spider plot – REE chondrite (Boynton,1984)
C Group 2
Spider plot – Primitive Mantle (Sun and McDonough,1989)
D Group 2
Spider plot – REE chondrite (Boynton,1984)
E Group 3
Spider plot – Primitive Mantle (Sun and McDonough,1989)
F Group 3
Spider plot – REE chondrite (Boynton,1984)
G Sample 355
Spider plot – Primitive Mantle (Sun and McDonough,1989)
H Sample 355
Sample/ REE chondrite
Sample/ Primitive Mantle
La Ce Pr Nd Pm Sm Eu Gd Tb Dy Ho Er Tm Yb Lu
Cs Rb Ba Th U Nb K La Ce Pb Pr Sr P Nd Zr Sm Eu Ti Dy Y Yb Lu

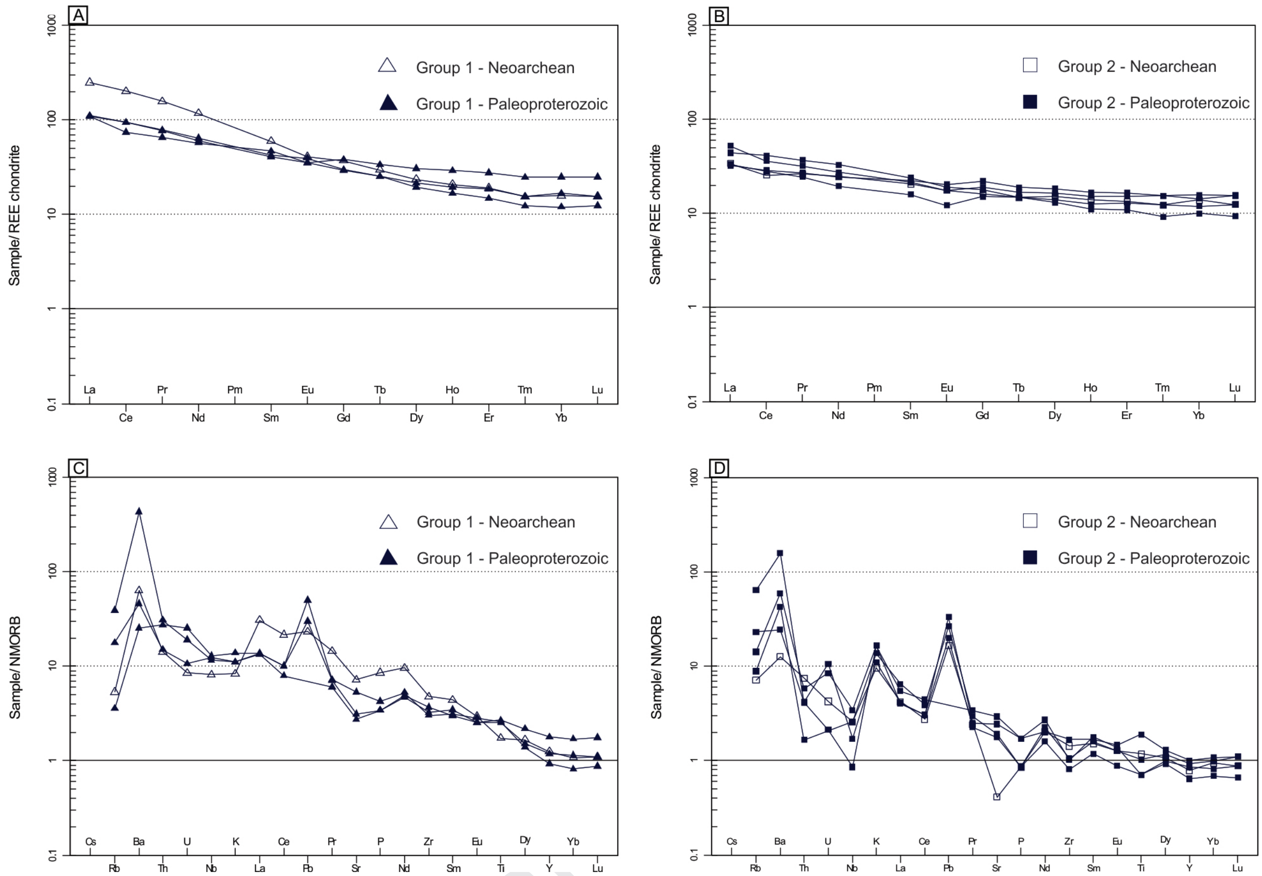
A
Group 1 - Neoarchean
Group 1 - Paleoproterozoic
Sample/ REE chondrite
B
Group 2 - Neoarchean
Group 2 - Paleoproterozoic
Sample/ REE chondrite
C
Group 1 - Neoarchean
Group 1 - Paleoproterozoic
Sample/ NMORB
D
Group 2 - Neoarchean
Group 2 - Paleoproterozoic
Sample/ NMORB

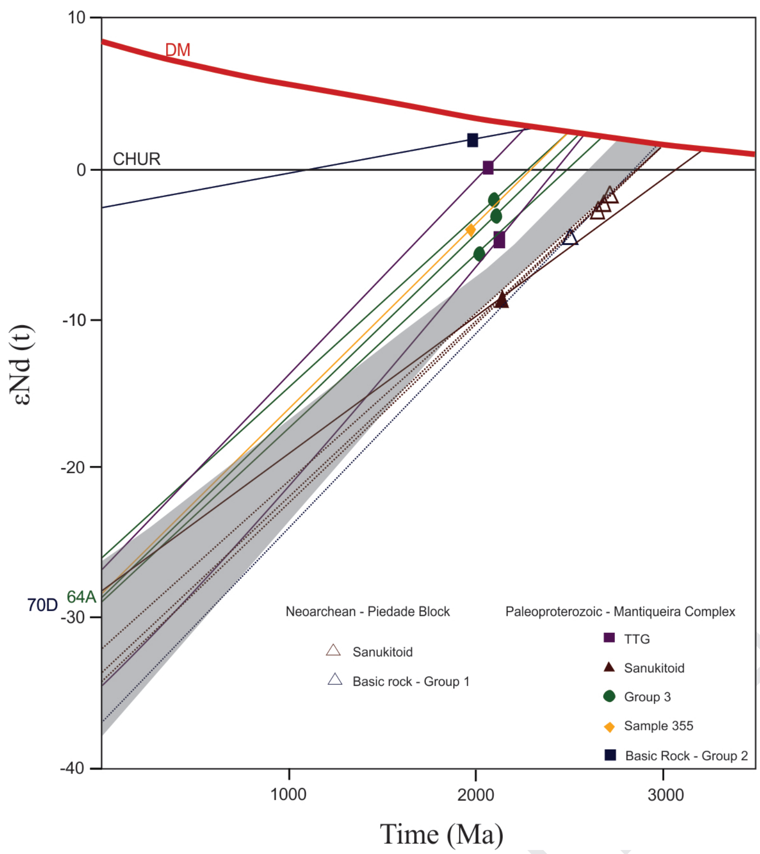

10
0
-10
-20
-30
-40
DM
CHUR
70D
64A
εNd (t)
1000
2000
3000
Time (Ma)
Neoarchean - Piedade Block
Sanukitoid
Basic rock - Group 1
Paleoproterozoic - Mantiqueira Complex
TTG
Sanukitoid
Group 3
Sample 355
Basic Rock - Group 2

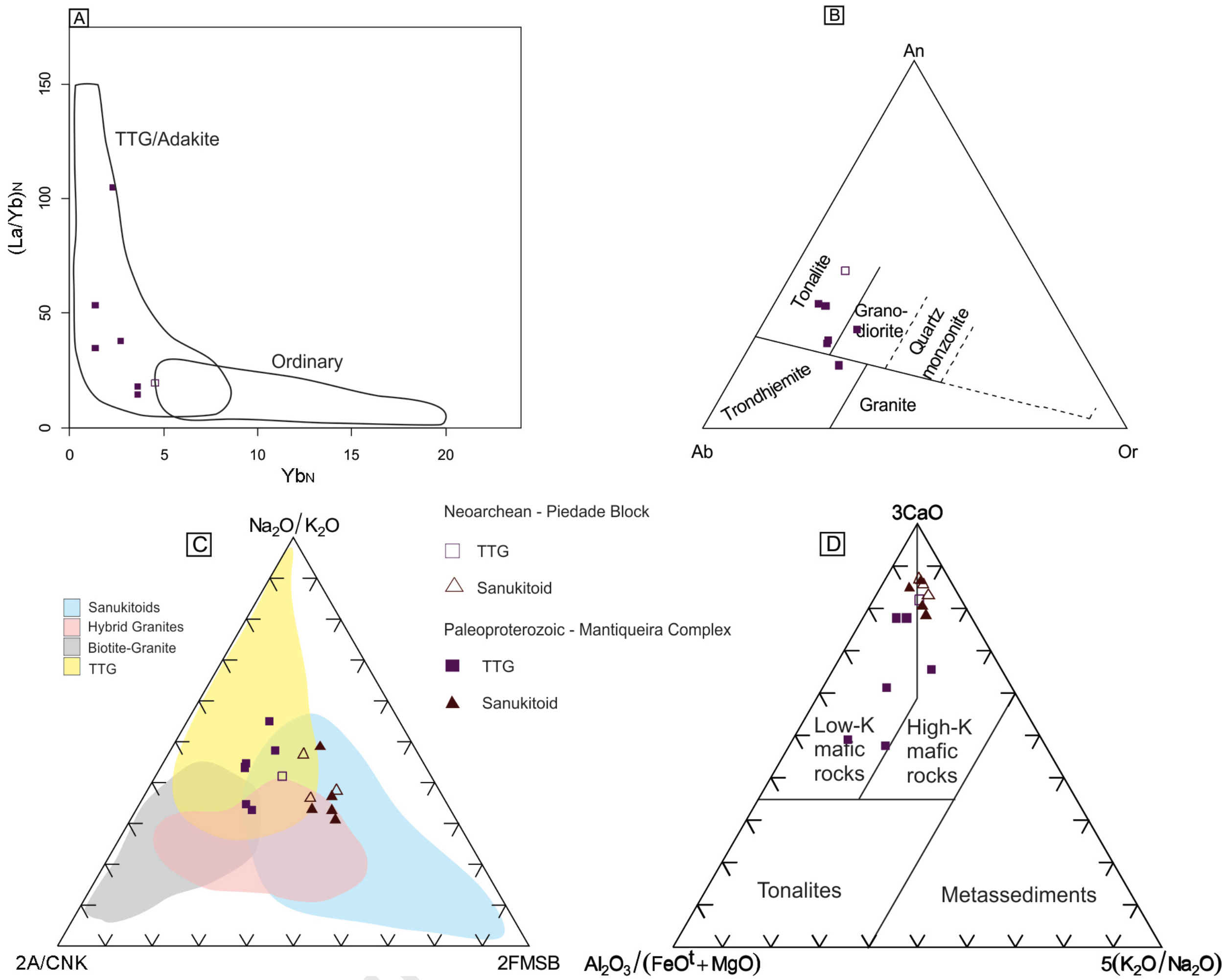
A
(La/Yb)N
YbN
TTG/Adakite
Ordinary
0
50
100
150
0
5
10
15
20
B
An
Ab
Or
Tonalite
Grano-
diorite
Quartz
monzonite
Trondhjemite
Granite
C
Na_2O/K_2O
2A/CNK
2FMSB
Sanukitoids
Hybrid Granites
Biotite-Granite
TTG
Neoarchean - Piedade Block
TTG
Sanukitoid
Paleoproterozoic - Mantiqueira Complex
TTG
Sanukitoid
D
3CaO
$Al_2O_3/(FeO^t+MgO)$
$5(K_2O/Na_2O)$
Low-K
mafic
rocks
High-K
mafic
rocks
Tonalites
Metassediments

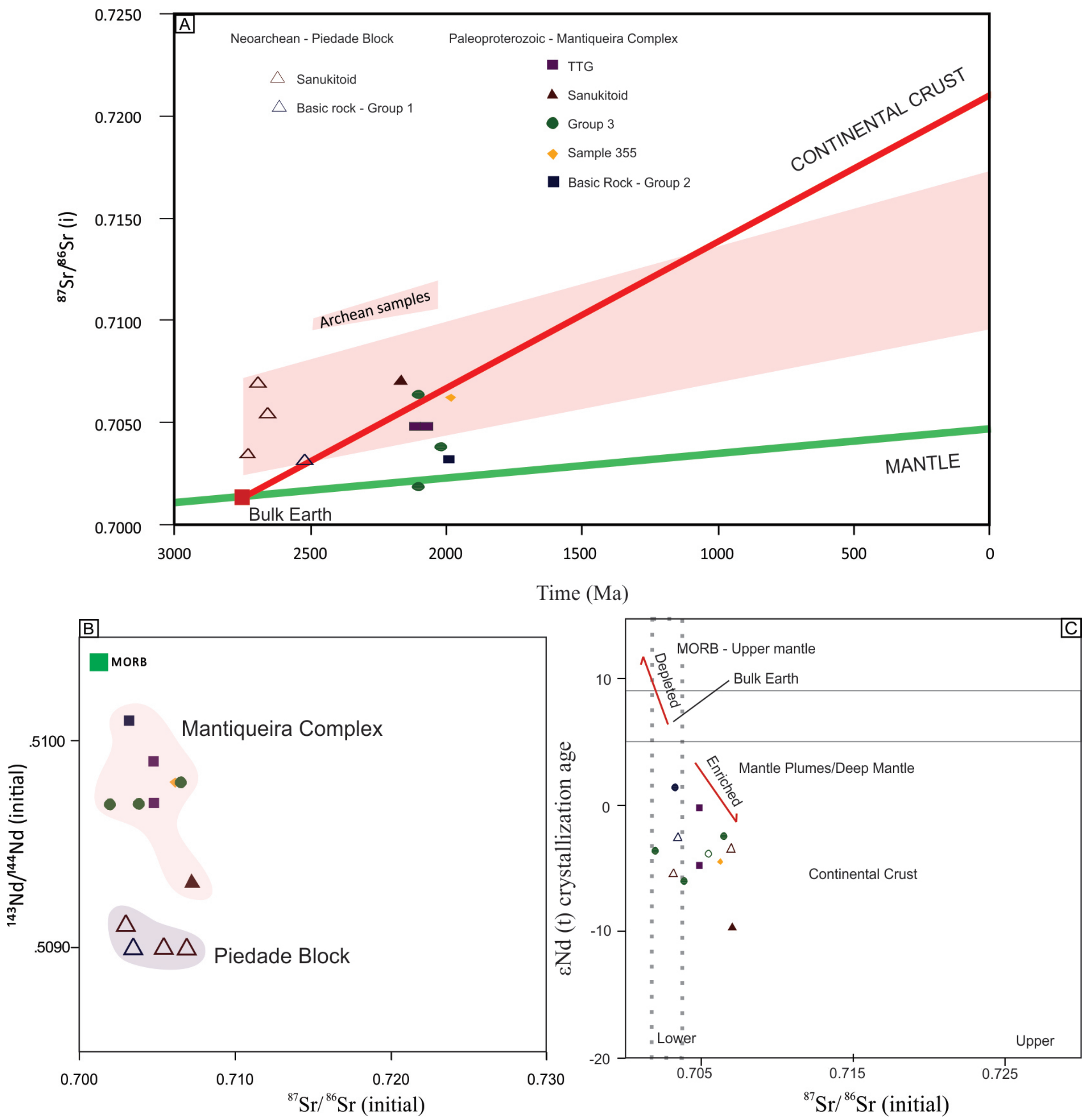
A
Neoarchean - Piedade Block
Sanukitoid
Basic rock - Group 1
Paleoproterozoic - Mantiqueira Complex
TTG
Sanukitoid
Group 3
Sample 355
Basic Rock - Group 2
CONTINENTAL CRUST
Archean samples
MANTLE
Bulk Earth
87Sr/86Sr (i)
0.7250
0.7200
0.7150
0.7100
0.7050
0.7000
3000
2500
2000
1500
1000
500
0
Time (Ma)
B
MORB
Mantiqueira Complex
Piedade Block
143Nd/144Nd (initial)
.5100
.5090
0.700
0.710
0.720
0.730
87Sr/86Sr (initial)
C
MORB - Upper mantle
Bulk Earth
Depleted
Enriched
Mantle Plumes/Deep Mantle
Continental Crust
Lower
Upper
εNd (t) crystallization age
10
0
-10
-20
0.705
0.715
0.725
87Sr/86Sr (initial)

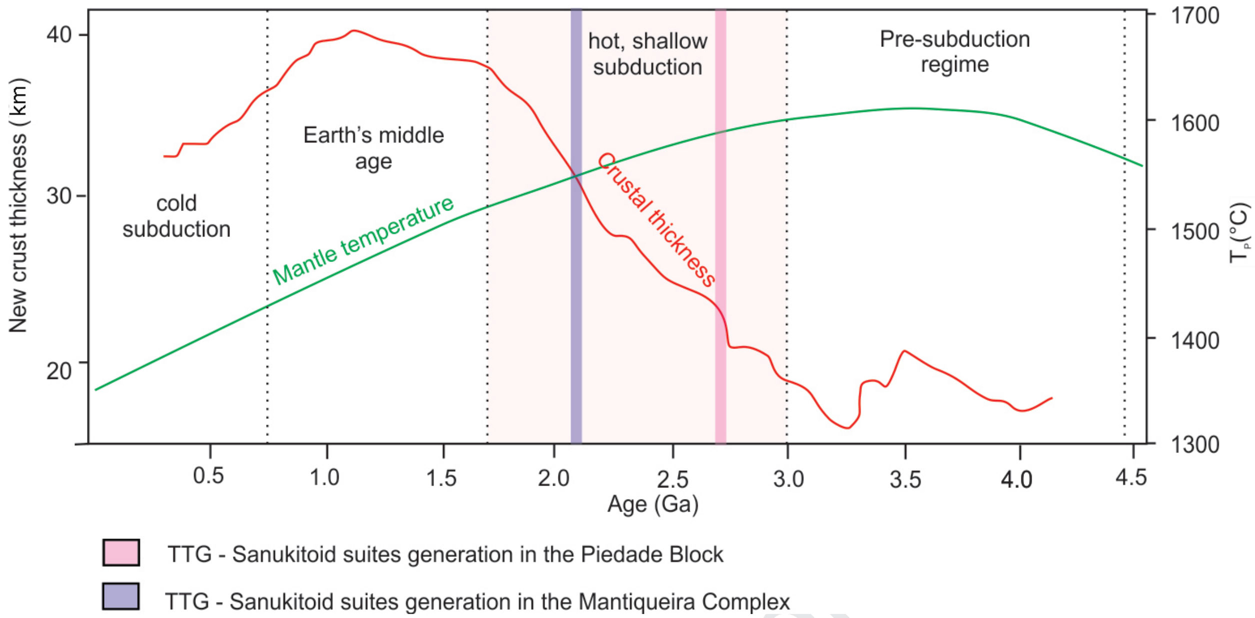

40
30
20
New crust thickness (km)
1700
1600
1500
1400
1300
T_P(°C)
0.5
1.0
1.5
2.0
2.5
3.0
3.5
4.0
4.5
Age (Ga)
cold subduction
Earth's middle age
hot, shallow subduction
Pre-subduction regime
Mantle temperature
Crustal thickness
TTG - Sanukitoid suites generation in the Piedade Block
TTG - Sanukitoid suites generation in the Mantiqueira Complex

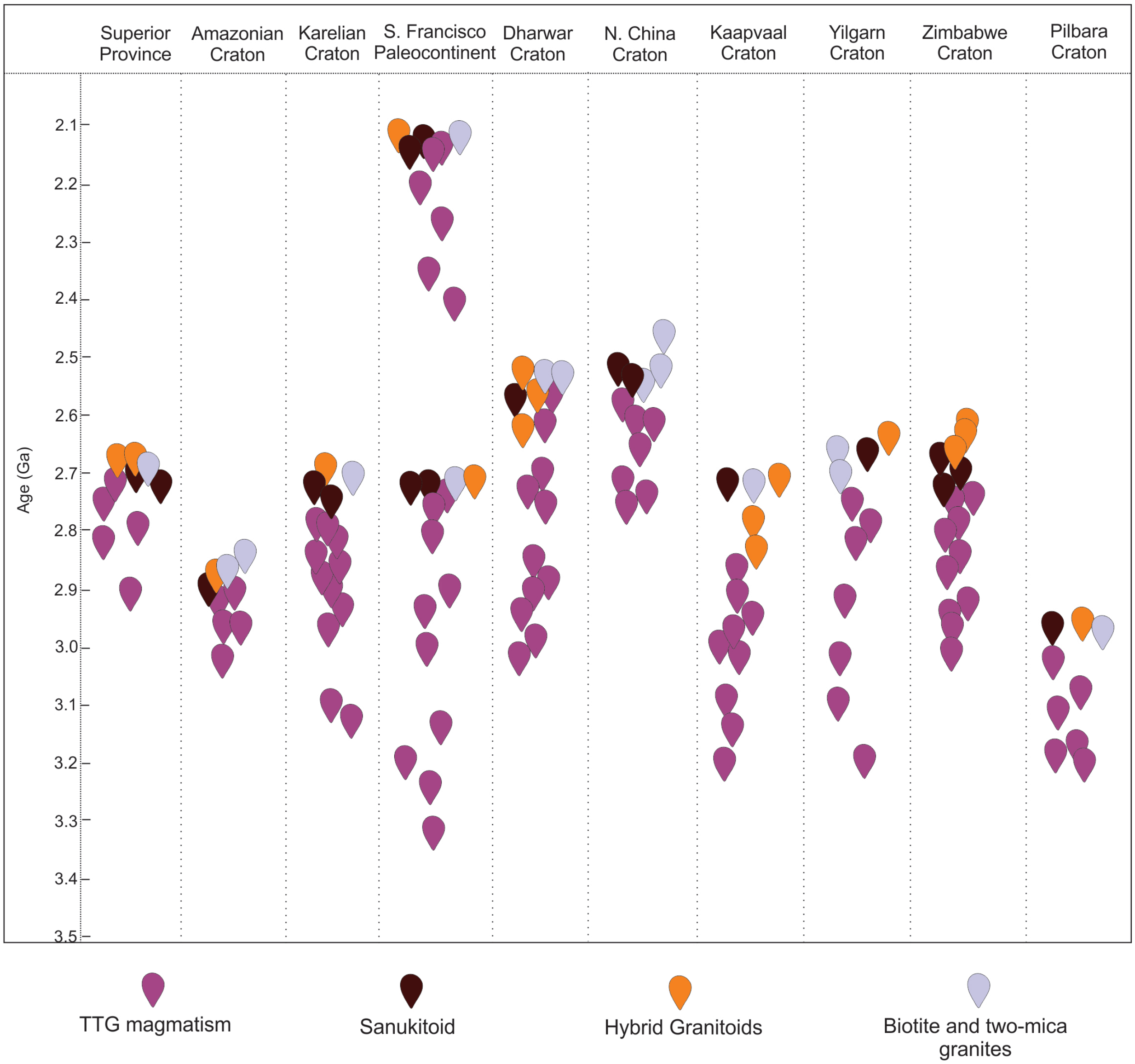

Superior Province
Amazonian Craton
Karelian Craton
S. Francisco Paleocontinent
Dharwar Craton
N. China Craton
Kaapvaal Craton
Yilgarn Craton
Zimbabwe Craton
Pilbara Craton
Age (Ga)
2.1
2.2
2.3
2.4
2.5
2.6
2.7
2.8
2.9
3.0
3.1
3.2
3.3
3.4
3.5
TTG magmatism
Sanukitoid
Hybrid Granitoids
Biotite and two-mica granites

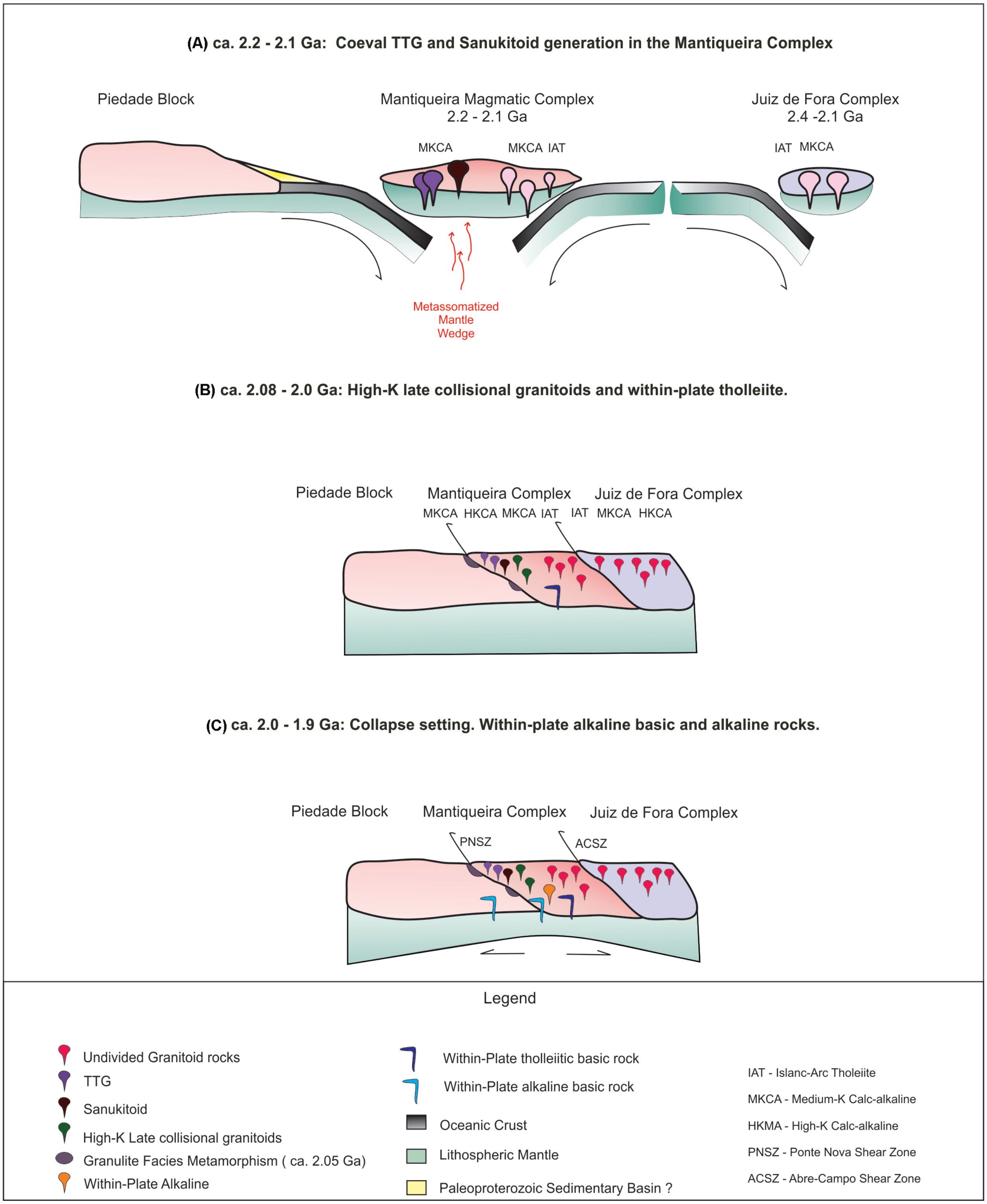
(A) ca. 2.2 - 2.1 Ga: Coeval TTG and Sanukitoid generation in the Mantiqueira Complex
Piedade Block
Mantiqueira Magmatic Complex
2.2 - 2.1 Ga
Juiz de Fora Complex
2.4 -2.1 Ga
MKCA
MKCA IAT
IAT MKCA
Metassomatized
Mantle
Wedge
(B) ca. 2.08 - 2.0 Ga: High-K late collisional granitoids and within-plate tholleiite.
Piedade Block
Mantiqueira Complex
Juiz de Fora Complex
MKCA HKCA MKCA IAT
IAT MKCA HKCA
(C) ca. 2.0 - 1.9 Ga: Collapse setting. Within-plate alkaline basic and alkaline rocks.
Piedade Block
Mantiqueira Complex
Juiz de Fora Complex
PNSZ
ACSZ
Legend
Undivided Granitoid rocks
TTG
Sanukitoid
High-K Late collisional granitoids
Granulite Facies Metamorphism (ca. 2.05 Ga)
Within-Plate Alkaline
Within-Plate tholleiitic basic rock
Within-Plate alkaline basic rock
Oceanic Crust
Lithospheric Mantle
Paleoproterozoic Sedimentary Basin ?
IAT - Islanc-Arc Tholeiite
MKCA - Medium-K Calc-alkaline
HKMA - High-K Calc-alkaline
PNSZ - Ponte Nova Shear Zone
ACSZ - Abre-Campo Shear Zone

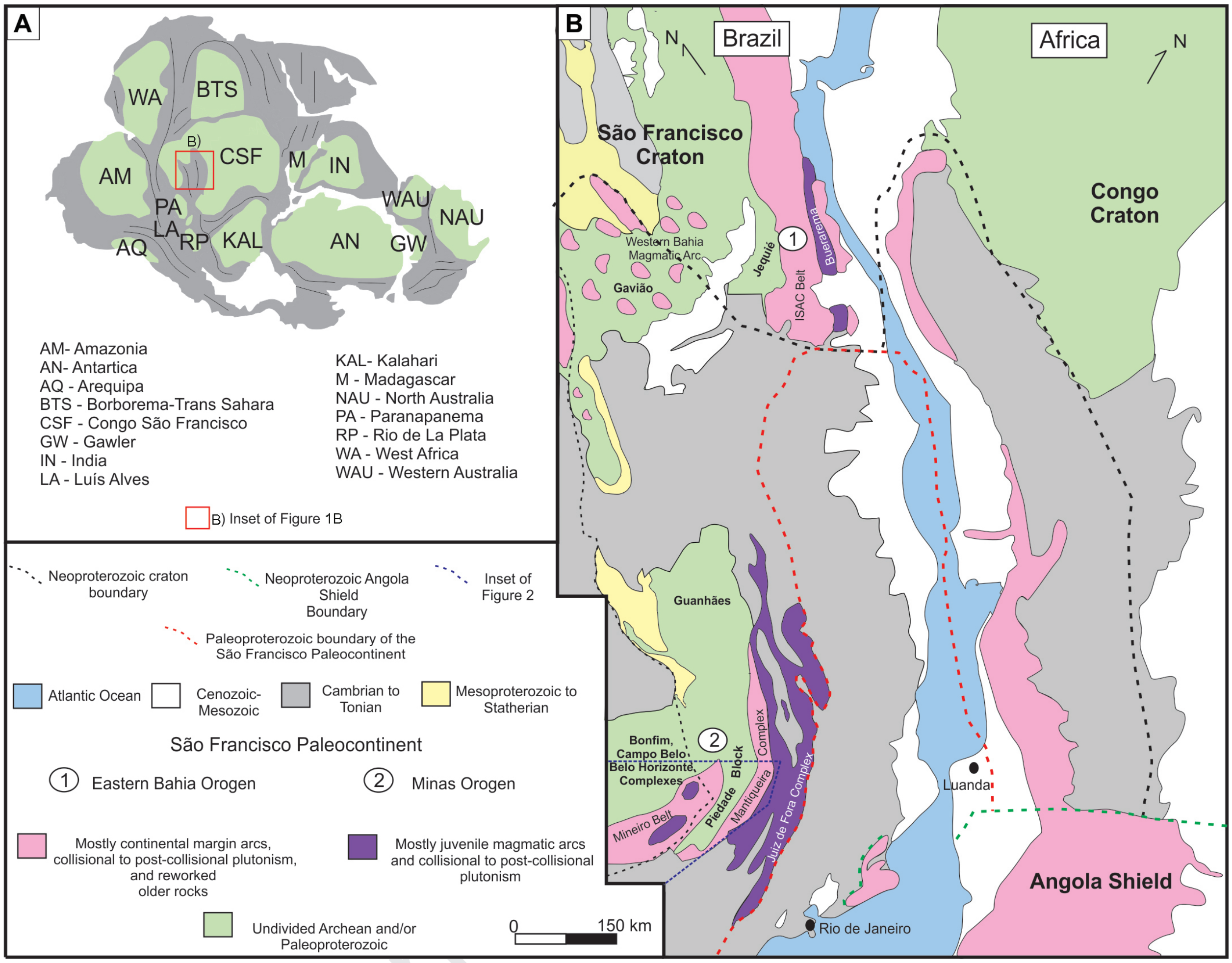
A
WA
BTS
B)
CSF
M
IN
AM
PA
LA
RP
KAL
AQ
AN
WAU
NAU
GW
AM- Amazonia
AN- Antartica
AQ - Arequipa
BTS - Borborema-Trans Sahara
CSF - Congo São Francisco
GW - Gawler
IN - India
LA - Luís Alves
KAL- Kalahari
M - Madagascar
NAU - North Australia
PA - Paranapanema
RP - Rio de La Plata
WA - West Africa
WAU - Western Australia
B) Inset of Figure 1B
Neoproterozoic craton boundary
Neoproterozoic Angola Shield Boundary
Inset of Figure 2
Paleoproterozoic boundary of the São Francisco Paleocontinent
Atlantic Ocean
Cenozoic-Mesozoic
Cambrian to Tonian
Mesoproterozoic to Statherian
São Francisco Paleocontinent
1 Eastern Bahia Orogen
2 Minas Orogen
Mostly continental margin arcs, collisional to post-collisional plutonism, and reworked older rocks
Mostly juvenile magmatic arcs and collisional to post-collisional plutonism
Undivided Archean and/or Paleoproterozoic
0 150 km
B
N
Brazil
Africa
N
São Francisco Craton
Congo Craton
Western Bahia Magmatic Arc
Gavião
Jequié
ISAC Belt
Buerarema
1
Guanhães
Bonfim, Campo Belo Belo Horizonte Complexes
2
Mineiro Belt
Piedade Block
Mantiqueira Complex
Juiz de Fora Complex
Luanda
Rio de Janeiro
Angola Shield

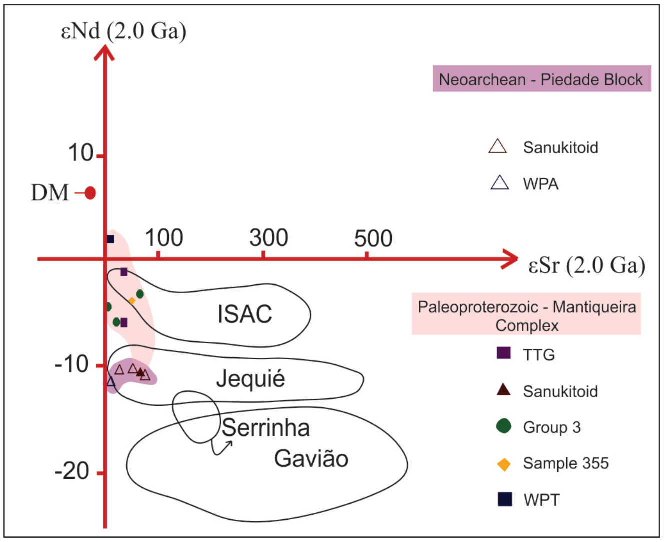

εNd (2.0 Ga)
Neoarchean - Piedade Block
Sanukitoid
WPA
10
DM
100
300
500
εSr (2.0 Ga)
ISAC
Paleoproterozoic - Mantiqueira Complex
TTG
-10
Jequié
Sanukitoid
Group 3
Serrinha
Gavião
-20
Sample 355
WPT

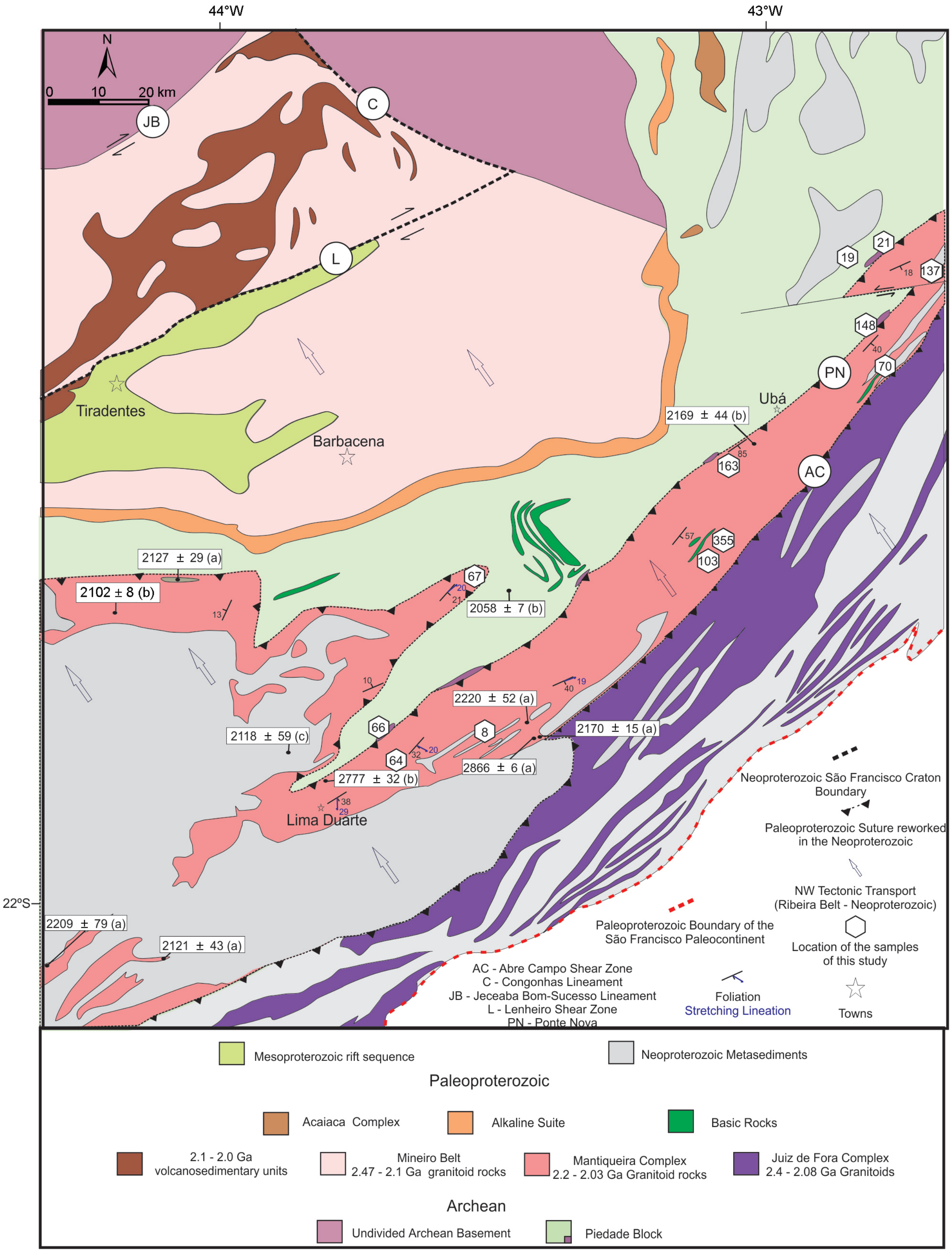
44°W
43°W
22°S
N
0 10 20 km
JB
C
L
PN
AC
Tiradentes
Barbacena
Ubá
Lima Duarte
2127 ± 29 (a)
2102 ± 8 (b)
2058 ± 7 (b)
2169 ± 44 (b)
2220 ± 52 (a)
2118 ± 59 (c)
2170 ± 15 (a)
2777 ± 32 (b)
2866 ± 6 (a)
2209 ± 79 (a)
2121 ± 43 (a)
19
21
137
148
70
163
355
103
67
66
64
8
Neoproterozoic São Francisco Craton Boundary
Paleoproterozoic Suture reworked in the Neoproterozoic
NW Tectonic Transport (Ribeira Belt - Neoproterozoic)
Paleoproterozoic Boundary of the São Francisco Paleocontinent
Location of the samples of this study
AC - Abre Campo Shear Zone
C - Congonhas Lineament
JB - Jeceaba Bom-Sucesso Lineament
L - Lenheiro Shear Zone
PN - Ponte Nova
Foliation
Stretching Lineation
Towns
Mesoproterozoic rift sequence
Neoproterozoic Metasediments
Paleoproterozoic
Acaiaca Complex
Alkaline Suite
Basic Rocks
2.1 - 2.0 Ga volcanosedimentary units
Mineiro Belt 2.47 - 2.1 Ga granitoid rocks
Mantiqueira Complex 2.2 - 2.03 Ga Granitoid rocks
Juiz de Fora Complex 2.4 - 2.08 Ga Granitoids
Archean
Undivided Archean Basement
Piedade Block


A
B
C
D
E
F

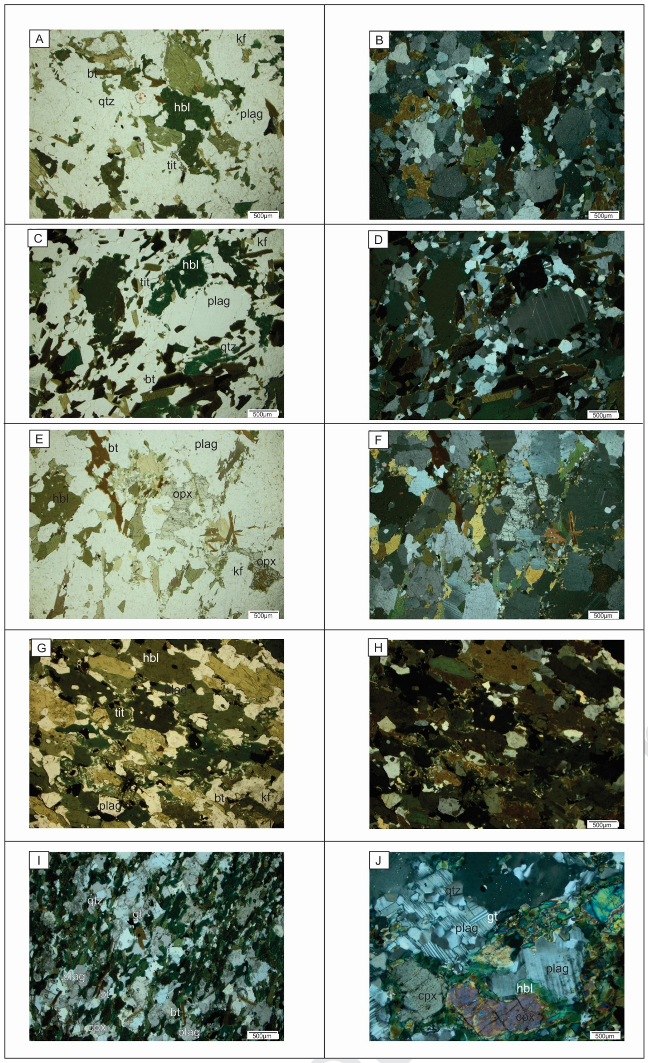
A
kf
bt
qtz
hbl
plag
tit
B
C
kf
hbl
tit
plag
qtz
bt
D
E
bt
plag
hbl
opx
kf
opx
F
G
hbl
tit
plag
bt
kf
H
I
qtz
gt
plag
bt
opx
plag
J
qtz
gt
plag
plag
cpx
hbl
opx


A Sample 66A
20µm
207Pb/206Pb - 2683 ± 11
Th/U - 0.07
Conc: 97%
Spot #26
207Pb/206Pb - 2690 ± 9
Th/U - 0.69
Conc: 99%
Spot #29
207Pb/206Pb - 2724 ± 15
Th/U - 0.23
Conc: 100%
Spot #18
207Pb/206Pb - 2034 ± 25
Th/U - 0.94
Conc: 95%
Spot #27
207Pb/206Pb - 2716± 9
Th/U - 0.5
Conc: 89%
Spot #28
B Sample 66B
207Pb/206Pb - 2571± 20
Th/U - 0.57
99%
Spot #36
20µm
207Pb/206Pb - 2689± 10
Th/U - 0.68
Conc: 99%
Spot #45
207Pb/206Pb - 2582± 14
Th/U - 0.58
Conc: 97%
Spot #39
30µm
207Pb/206Pb - 2008 ± 28
Th/U - 1.03
Conc: 100%
Spot #37
20µm
207Pb/206Pb - 1990 ± 28
Th/U - 0.38
Conc: 100%
Spot #46
207Pb/206Pb - 2013 ± 35
Th/U - 0.34
Conc: 98%
Spot #39
C Sample 21A
207Pb/206Pb - 2518 ± 17
Th/U - 1.80
Spot #112
207Pb/206Pb - 2688 ± 17
Th/U - 1.64
Spot #41
207Pb/206Pb - 2536 ± 17
Th/U - 1.39
Spot #74
207Pb/206Pb - 2500 ± 17
Th/U - 1.55
Spot #75
100µm
D Sample 21B
207Pb/206Pb - 2628 ± 24
Th/U - 1.26
Spot #39
207Pb/206Pb - 2039 ± 26
Th/U - 1.18
Spot #49
207Pb/206Pb - 2627 ± 23
Th/U - 1.25
Spot #14
207Pb/206Pb - 3065 ± 23
Th/U - 0.77
Spot #67
E Sample 148
207Pb/206Pb - 2659 ± 23
Th/U - 0.60
Spot #14
207Pb/206Pb - 2085 ± 38
Th/U - 0.51
Spot #49
207Pb/206Pb - 2589 ± 24
Th/U - 0.44
Spot #48
207Pb/206Pb - 2619 ± 23
Th/U - 0.39
Spot #10
100µm
F Sample 19A
206Pb/238U - 880 ± 19
Th/U - 0.22
Spot #195
207Pb/206Pb - 2706 ± 24
Th/U - 0.58
Spot #172
207Pb/206Pb - 2662 ± 20
Th/U - 0.56
Spot #219
100µm
G Sample 19B
100µm
207Pb/206Pb - 1974 ± 19
Th/U - 1.18
Spot #38
207Pb/206Pb - 1938 ± 19
Th/U - 0.89
Spot #125
207Pb/206Pb - 3045 ± 17
Th/U - 0.73
Spot #88
207Pb/206Pb - 3172 ± 16
Th/U - 1.19
Spot #87
207Pb/206Pb - 2626 ± 17
Th/U - 0.46
Spot #124
207Pb/206Pb - 2547 ± 26
Th/U - 0.76
Spot #37

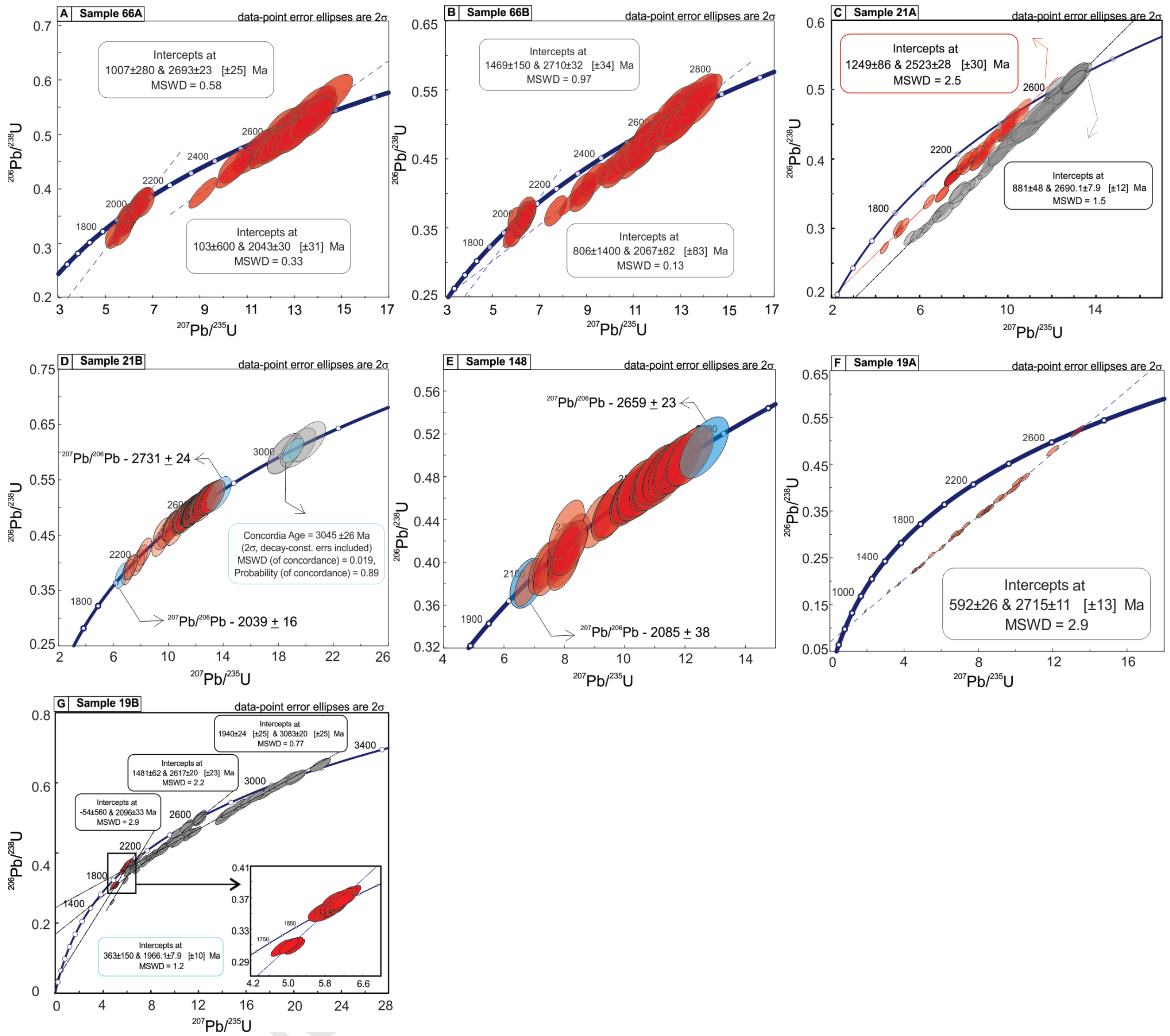
A Sample 66A
data-point error ellipses are 2σ
Intercepts at
1007±280 & 2693±23 [±25] Ma
MSWD = 0.58
Intercepts at
103±600 & 2043±30 [±31] Ma
MSWD = 0.33
B Sample 66B
data-point error ellipses are 2σ
Intercepts at
1469±150 & 2710±32 [±34] Ma
MSWD = 0.97
Intercepts at
806±1400 & 2067±82 [±83] Ma
MSWD = 0.13
C Sample 21A
data-point error ellipses are 2σ
Intercepts at
1249±86 & 2523±28 [±30] Ma
MSWD = 2.5
Intercepts at
881±48 & 2690.1±7.9 [±12] Ma
MSWD = 1.5
D Sample 21B
data-point error ellipses are 2σ
207Pb/206Pb - 2731 ± 24
Concordia Age = 3045 ±26 Ma
(2σ, decay-const. errs included)
MSWD (of concordance) = 0.019,
Probability (of concordance) = 0.89
207Pb/206Pb - 2039 ± 16
E Sample 148
data-point error ellipses are 2σ
207Pb/206Pb - 2659 ± 23
207Pb/206Pb - 2085 ± 38
F Sample 19A
data-point error ellipses are 2σ
Intercepts at
592±26 & 2715±11 [±13] Ma
MSWD = 2.9
G Sample 19B
data-point error ellipses are 2σ
Intercepts at
1940±24 [±25] & 3083±20 [±25] Ma
MSWD = 0.77
Intercepts at
1481±62 & 2617±20 [±23] Ma
MSWD = 2.2
Intercepts at
-54±560 & 2096±33 Ma
MSWD = 2.9
Intercepts at
363±150 & 1966.1±7.9 [±10] Ma
MSWD = 1.2
206Pb/238U
207Pb/235U

A Sample 08
207Pb/206Pb - 2037 ± 38
Th/U - 0.2
Conc: 91%
Spot #9
20µm
206Pb/238U - 576 ± 13
Th/U - 0.02
Conc: 100%
Spot #6
207Pb/206Pb - 1986 ± 45
Th/U - 0.45
Conc:: 88%
Spot #25
207Pb/206Pb - 2075 ± 81
Th/U - 0.54
Conc: 89%
Spot #6
206Pb/238U - 576 ± 12
Th/U - 0.02
Conc: 99%
Spot #10
30µm
20µm
B Sample 67
207Pb/206Pb - 2115 ± 17
Th/U - 0.25
Conc: 95%
Spot #15
207Pb/206Pb - 1951 ± 16
Th/U - 0.03
Conc: 85%
Spot #29
207Pb/206Pb - 2089 ± 18
Th/U - 0.25
Conc: 98%
Spot #17
20µm
207Pb/206Pb - 1963 ± 18
Th/U - 0.08
Conc: 79%
Spot #18
207Pb/206Pb - 2046 ± 18
Th/U - 0.03
Conc: 94%
Spot #14
30µm
20µm
C Sample 163A
50µm
207Pb/206Pb - 2098 ± 26
Th/U - 0.82
Spot #114
206Pb/238U - 582 ± 15
Th/U - 0.75
Spot #47
207Pb/206Pb - 2012 ± 25
Th/U - 0.64
Spot #97
D Sample 137G
207Pb/206Pb - 2024 ± 27
Th/U - 0.72
Spot #132
206Pb/238U - 565 ± 14
Th/U - 0.15
Spot #200
207Pb/206Pb - 2008 ± 26
Th/U - 0.68
Spot #131
40µm
40µm
40µm
E Sample 64A
207Pb/206Pb - 1795 ± 28
Th/U - 0.41
Conc: 83%
Spot #35
207Pb/206Pb - 2069 ± 22
Th/U - 0.30
Conc: 95%
Spot #29
207Pb/206Pb - 1975 ± 24
Th/U - 0.16
Conc: 92%
Spot #2
207Pb/206Pb - 2047 ± 12
Th/U - 0.17
Conc: 93%
Spot #16
30µm
20µm
20µm
206Pb/238U - 572 ± 44
Th/U - 0.02
Conc: 100%
Spot #15
20µm
207Pb/206Pb - 2067 ± 15
Th/U - 0.22
Conc: 95%
Spot #34
206Pb/238U - 576 ± 44
Th/U - 0.02
Conc: 100%
Spot #2
F Sample 64B
207Pb/206Pb - 606 ± 11
Th/U - 0.02
Conc: 100%
Spot #3
206Pb/238U - 589 ± 13
Th/U - 0.03
Conc: 100%
Spot #14
207Pb/206Pb - 2032 ± 69
Th/U - 0.47
Conc: 100%
Spot #17
20µm
20µm
20µm
207Pb/206Pb - 2030 ± 62
Th/U - 0.31
Conc: 89%
Spot #13
207Pb/206Pb - 2055 ± 45
Th/U - 0.87
Conc: 97%
Spot #18
207Pb/206Pb - 1932 ± 61
Th/U - 0.79
Conc: 81%
Spot #1
G Sample 355
207Pb/206Pb - 2022 ± 25
Th/U - 0.80
Spot #75
206Pb/238U - 548 ± 13
Th/U - 0.11
Spot #69
207Pb/206Pb - 1958 ± 27
Th/U - 0.71
Spot #78
30µm
30µm
H Sample 103C
50µm
50µm
50µm
207Pb/206Pb - 2035 ± 18
Th/U - 0.71
Spot #42
207Pb/206Pb - 2036 ± 21
Th/U - 1.67
Spot #18
207Pb/206Pb - 2044 ± 18
Th/U - 0.81
Spot #30
H Sample 70D
207Pb/206Pb - 1982 ± 28
Th/U - 4.5
Spot #58
206Pb/238U - 594 ± 13
Th/U - 0.36
Spot #7
207Pb/206Pb - 1999 ± 27
Th/U - 1.21
Spot #40
30µm
30µm
30µm

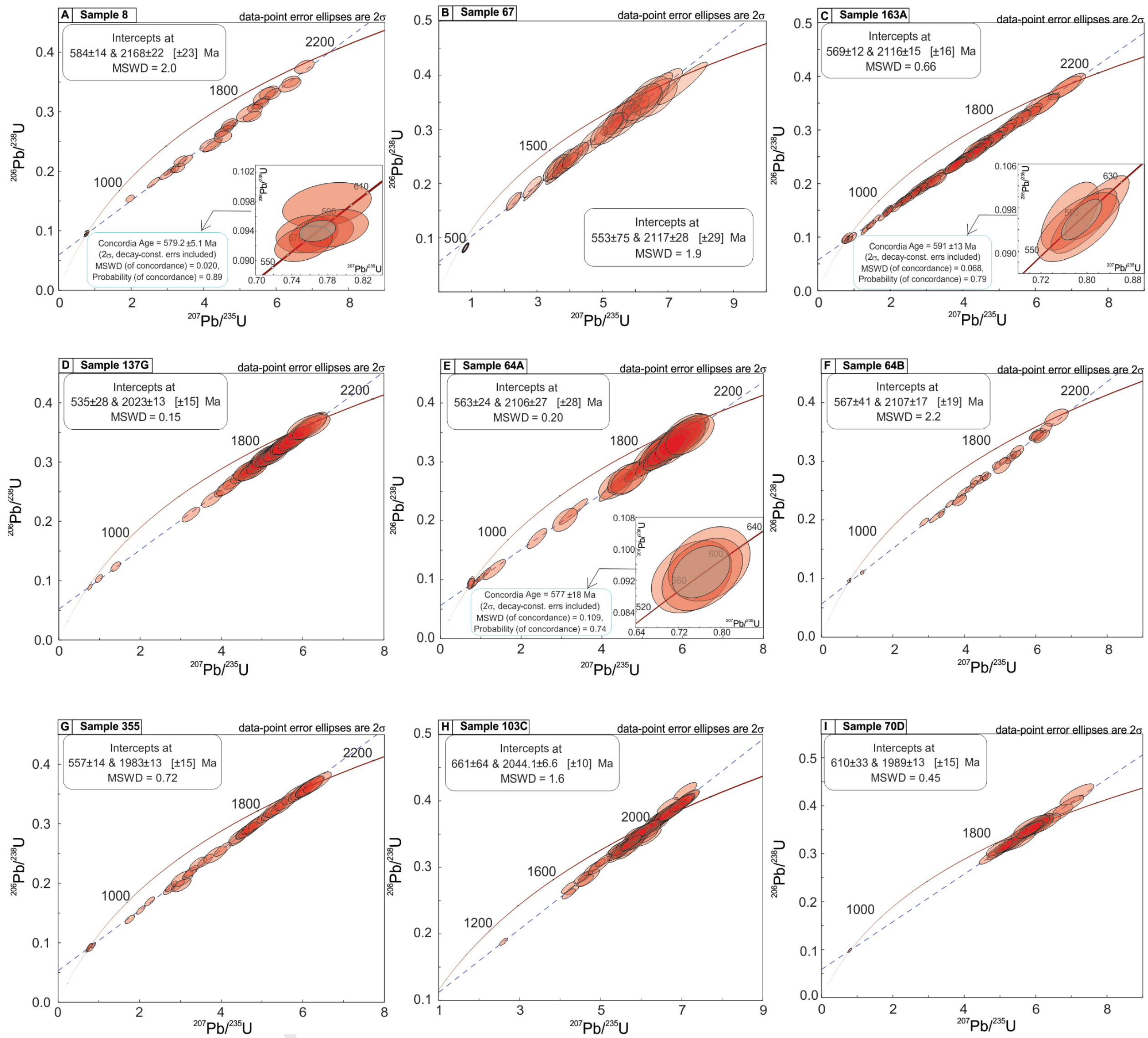
A Sample 8
data-point error ellipses are 2σ
Intercepts at
584±14 & 2168±22 [±23] Ma
MSWD = 2.0
Concordia Age = 579.2 ±5.1 Ma
(2σ, decay-const. errs included)
MSWD (of concordance) = 0.020,
Probability (of concordance) = 0.89
B Sample 67
Intercepts at
553±75 & 2117±28 [±29] Ma
MSWD = 1.9
C Sample 163A
Intercepts at
569±12 & 2116±15 [±16] Ma
MSWD = 0.66
Concordia Age = 591 ±13 Ma
(2σ, decay-const. errs included)
MSWD (of concordance) = 0.068,
Probability (of concordance) = 0.79
D Sample 137G
Intercepts at
535±28 & 2023±13 [±15] Ma
MSWD = 0.15
E Sample 64A
Intercepts at
563±24 & 2106±27 [±28] Ma
MSWD = 0.20
Concordia Age = 577 ±18 Ma
(2σ, decay-const. errs included)
MSWD (of concordance) = 0.109,
Probability (of concordance) = 0.74
F Sample 64B
Intercepts at
567±41 & 2107±17 [±19] Ma
MSWD = 2.2
G Sample 355
Intercepts at
557±14 & 1983±13 [±15] Ma
MSWD = 0.72
H Sample 103C
Intercepts at
661±64 & 2044.1±6.6 [±10] Ma
MSWD = 1.6
I Sample 70D
Intercepts at
610±33 & 1989±13 [±15] Ma
MSWD = 0.45
206Pb/238U
207Pb/235U

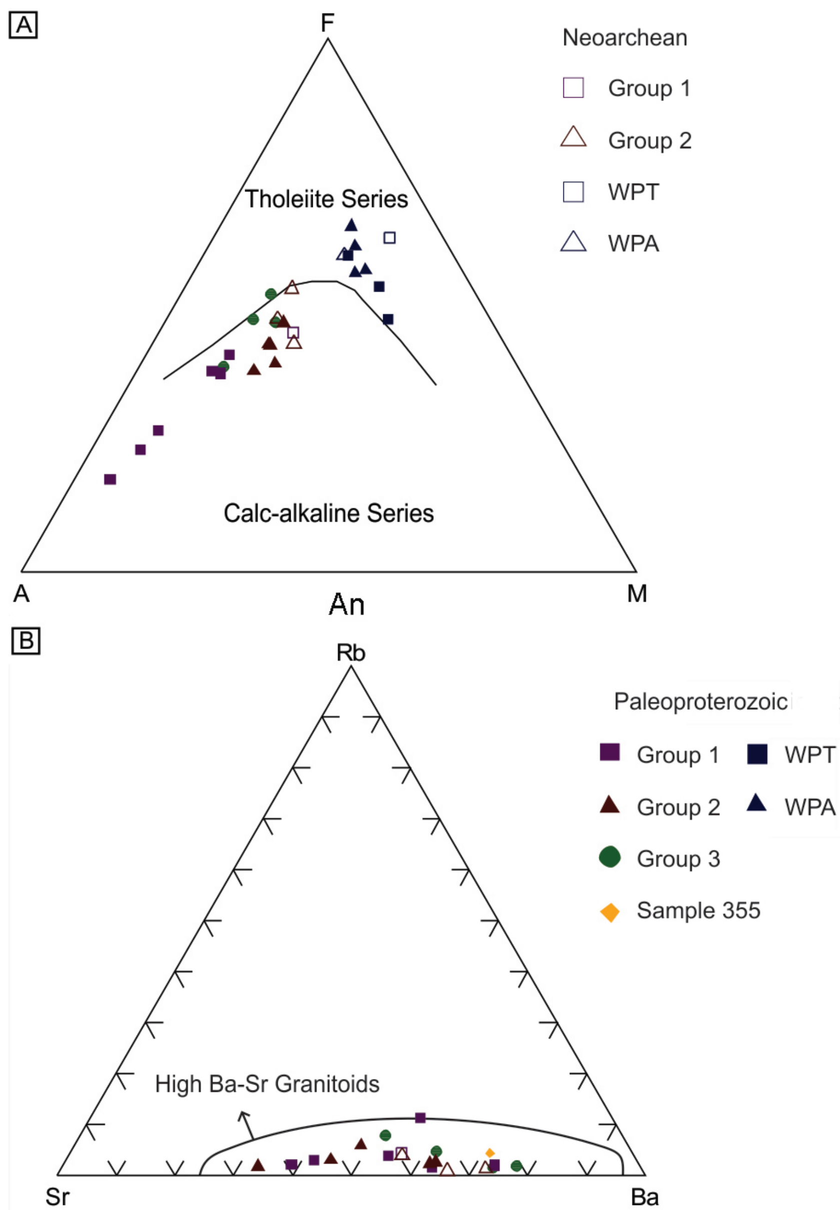
A
F
Neoarchean
Group 1
Group 2
WPT
WPA
Tholeiite Series
Calc-alkaline Series
A
An
M
B
Rb
Paleoproterozoic
Group 1
WPT
Group 2
WPA
Group 3
Sample 355
High Ba-Sr Granitoids
Sr
Ba

Highlights

- Diachronous TTG-sanukitoid transition in the southern São Francisco Paleocontinent.
- Mantiqueira Complex and Piedade Block form distinct tectonostratigraphic terranes.
- Geochemically and isotopically contrasting terranes juxtaposed during the Rhyacian.
- Complete orogenic cycle recorded in the Piedade Block and the Mantiqueira Complex.
- U-Pb in zircon, whole-rock Sm-Nd, Sr-Rb and lithogeochemistry analyses.

Declaration of interests

The authors declare that they have no known competing financial interests or personal relationships that could have appeared to influence the work reported in this paper.